Effect of two-phase gas-liquid flow patterns on cuttings transport efficiency.

SALUBI, V., MAHON, R., OLUYEMI, G. and OYENEYIN, B.

2022

Effect of Two-phase Gas-Liquid Flow Patterns on Cuttings Transport Efficiency

Voke Salubi[a*], Ruissein Mahon[a*], Gbenga Oluyemi[a], Babs Oyeneyin[a**]

[a]School of Engineering, Robert Gordon University, Aberdeen, UK, AB10 7GJ

**Now retired

*Email: v.salubi@rgu.ac.uk (V. Salubi) and r.r.mahon@rgu.ac.uk (R. Mahon)

Abstract

Effective cuttings transport and accurate drilling hydraulics prediction remain issues of concern during drilling operations of horizontal, extended reach and multilateral wells. While several studies have adopted a two- or three-layered modelling approach to evaluate cuttings transport efficiency, they have neglected the effect of the gas-liquid fluid flow pattern within the annulus on cuttings transport. An experimental and theoretical study was carried out to evaluate the interplay between the two-phase gas-liquid flow patterns and the major drilling parameters and investigate its influence on the cuttings and fluid flow dynamics in a horizontal and inclined drilling wellbore. Several mathematical flow pattern dependent multi-layered models valid for any level of wellbore eccentricity were developed for the different cuttings transport mechanisms in the bubble, dispersed bubble, stratified and slug gas-liquid flow patterns, thereby providing a method to evaluate cuttings transport efficiency and perform wellbore hydraulics calculations for underbalanced drilling operations. Experimental results show that both fluid flow pattern and the drilling fluid flowrate are the most influential controllable parameters that affect the cuttings transport efficiency. Moreover, the hole cleaning requirements for an eccentric annulus is higher than that required for the concentric annulus of both single-phase and two-phase Newtonian or non-Newtonian fluids. Inclination angle was also found to influence hole cleaning and the degree of its effect is highly dependent on the fluid properties, the cutting transport mechanism and prevailing gas-liquid flow pattern. In the horizontal and inclined eccentric annuli, drillpipe rotation can improve cuttings transport for both single-phase and two-phase flows, but generally the effect of the drillpipe rotation on two-phase flow for cutting transport is much less than that of the single-phase flow. Overall, a good match was found between the mathematical flow pattern dependent multi-layered models and the experimental data. The findings of this study serve as a guide in the prediction of the wellbore dynamics for underbalanced drilling operations and provides a tool that can be applied for wellbore pressure management and the evaluation of hole cleaning based upon the specified flow conditions.

Keywords: Cuttings transport, Multiphase flow, Multi-layered model, Wellbore hydraulics, Gas-liquid flow patterns, Underbalanced drilling

1.0 Introduction

Drilling of complex structure wells in the oil and gas industry has been on the rise due to the increasing demand for crude oil (Ma et al., 2016). These complex structure wells such as horizontal wells, extended reach wells and multilateral wells are often used in order to enhance hydrocarbon recovery and optimise productivity (Verma et al., 2017). In depleted or low-pressure reservoirs, if the hydrostatic pressure is higher than the formation pressure, wellbore instability issues emerge, leading to lost circulation, formation damage, and pollution of the reservoir (Akhshik and Rajabi, 2018; Fadairo et al., 2020; Lim et al., 2015). Multiphase (gas-liquid) drilling fluids are mostly used in these environments to control the wellbore pressures and improve the stability and productivity of the field by reducing formation damage (Ostroot et al., 2007). The primary function of the drilling fluid is to transport the drilled cuttings effectively out of the wellbore, but the pressure loss prediction and tendency for the solids to remain entrained in the flow is challenging due to the complexity of multiphase flow and the transient flow patterns. An improper hole cleaning job can lead to increased torque and drag, lost circulation, weight stacking, increased hydraulic requirements, stuck pipe, wellbore instability and improper cementing jobs (Clark and Bickham, 1994).

Since the 1980s, a number of field and laboratory analyses have confirmed that effective cutting transport during an underbalanced drilling (UBD) operation is dependent on a number of important parameters. These include the prevailing flow pattern, the rheological properties of the drilling fluid, the pipe and wellbore/casing sizes, wellbore inclination angle, the cutting sizes, drillpipe rotary speeds, eccentricity and most importantly the fluid flowrates (Erge and van Oort, 2020; Gao and Young, 1995; Luo, 1988; Peden et al., 1990; Zhang et al., 2020). If the annular flowing velocity is not high enough to transport the cuttings, the cuttings would settle out of the flow and form a stationary bed thereby creating wellbore instability issues (Peden et al., 1990). It is therefore important to understand the hydraulics of multiphase flow and the manipulation of the key parameters in order to accurately predict the pressure losses and the optimal liquid/gas flowrates to ensure an effective hole-cleaning process.

Gavignet and Sobey (1989) presented a two-layered model to describe the motion of cuttings transport in deviated wellbores. The model was compared to the experimental data of Iyoho (1980) for both Newtonian and non-Newtonian fluids and was reported to favourably predict the increase in the cuttings concentration with wellbore inclination. They concluded that the criterion for the formation of a stationary bed in the wellbore annuli is highly dependent on the wellbore size, the cutting size and the degree of the drillpipe eccentricity.

Kamp and Rivero (1999) performed numerical simulations using a two-layered model approach to determine the cuttings transport velocities, pressure gradient and to predict the cuttings bed height while drilling at different flowrates and rates of penetration. They reported that the height of the bed formed in the annuli decreased with fluid flowrate and increased almost linearly with the rate of penetration (ROP).

Doan et al. (2000) modelled the transport of cuttings in UBD conditions as a two-phase flow process. They used three conservation of mass and momentum equations for the fluid phase and cuttings phase in a two-layered system. These equations were solved using a finite difference approach to generate results for a variety of hydrodynamic conditions, including fluid rheology, mud rate and viscosity, and cuttings size - after which they analysed and compared the results to experimental data. They found that the experimental results matched the numerically generated data and noted that the cuttings removal from the annuli is highly dependent on the cuttings injection rate. However, it was reported that the model prediction was poor when compared to experimental data for low cuttings injection rates.

Masuda et al. (2000) setup an experimental unit to investigate cuttings transport in inclined annuli to determine the critical flowrate required for an effective transport of drilled cuttings. Image analysis systems were applied to enable the estimation of the cuttings concentration and velocity. In order to simulate the transport of cuttings under UBD conditions, a transient numerical model was developed using a two-layer configuration, assuming the existence of a suspension and moving bed layer. The researchers compared their experimental results with numerical simulations and reported a favourable match for the majority of cases investigated. They concluded that the calculated cuttings velocity agreed with the measured cuttings velocity.

Cho et al. (2001) carried out a theoretical and experimental study to develop and test a method to predict cuttings transport efficiency and determine the frictional pressure losses experienced by the flow through deviated wellbores. A mathematical model was developed on the basis that the cuttings-drilling fluid flow creates a suspension and a stationary bed layer in the wellbore annuli. Conservation of mass equations were expressed for the cuttings and drilling fluid phase and momentum equations were derived for each of the layers assumed to exist in the annuli. Experiments were carried out to determine the cuttings volumetric concentration and the porosity of the cuttings bed. Their findings showed that additional frictional pressure losses were experienced due to the relative velocity between the cuttings and the drilling fluid in the bed layer. They therefore assumed that expressions used for flow through porous media can be applied to the cuttings bed layer. The researchers concluded that the flow of drilling fluid in a porous cuttings-bed had a significant effect on the pressure drop and a fluid with high viscosity will decrease the cuttings-bed size but increase the pressure gradient in the annuli. It was further recommended that an optimisation of the cuttings-bed size, pressure gradient, rheology of the fluid, and fluid flowrate is required to improve cuttings transport efficiency.

Li and Kuru (2004) developed a transient multiphase flow model in order to simulate the flow of cuttings with foam in horizontal wellbores. The idea behind this study was to determine the minimum velocity that ensures that no cuttings are deposited to form a bed in the annulus. This minimum velocity was defined as the critical foam velocity required to transport cuttings in a horizontal wellbore. They reported that the quality of the foam affects the cuttings transport efficiency due to its influence on the density and viscosity of the foam.

Li et al. (2007) presented a one-dimensional transient mechanistic model that is solved numerically to predict the height of the cuttings bed as a function of the circulation rate, drilling fluid rheology, ROP, drillpipe eccentricity and wellbore geometry. The two-layer modelling approach was applied with the assumption that there is a mass transfer process that occurs between the layers formed in the annuli. The cuttings were assumed to be spherical with uniform shapes and sizes and the slippage between the cuttings and the drilling fluid was taken into account. They compared the results obtained from the simulation with experimental data collected from the public domain and reported good agreement for drilling fluid flowrates less than 250 gpm. They concluded that the fluid flowrate is the most important factor governing cuttings transport and that a thicker mud will transport cuttings at lower fluid flowrates than that of a light mud or water.

Costa et al. (2008) investigated the effect of the ROP on the effectiveness of cuttings transport in the annuli. They also adopted the two-layer modelling approach with the assumption that the annuli space consists of a suspension and cuttings bed layer. The finite volume method was applied to discretise the governing mass and momentum partial differential equations combined with the Newton-Raphson technique. From the numerical solutions generated, it was concluded that ROP influences the bed formation and pressure distribution in the wellbore and the presented methodology was capable of evaluating the cuttings bed height, the cuttings concentrations, as well as, the pressure and equivalent circulating density (ECD) for an oil well drilling process.

As seen from the literature, a number of researchers have applied the two-layered modelling approach to evaluate the effectiveness of major drilling parameters on cuttings transport. Some studies have also reported the effectiveness of using the three-layered cutting transport modelling approach (Ozbayoglu et al., 2003; Wang et al., 2010). Apart from the multi-layered cutting transport modelling approach, other methods have been applied to provide a means to determine the optimum conditions required for cuttings transport during drilling. Analytical and emprical models fine tuned by experimental or numerical data have been developed and recommended (Duan et al., 2006; Luo, 1988; Okrajni and Azar, 1986; Ozbayoglu et al., 2007; Pandya et al., 2020; Wei et al., 2013). Recently, with the aid of computational fluid dynamics (CFD) techinques, some researchers have solved the governing fluid flow equations to obtain velocity and pressure fields along with the solution of mass and force balance equations for particle transport in the annuli geometry. These studies have employed such methods to investigate the influence of fluid rheology, drillpipe rotation, eccentricity, cutting properties, wellbore inclination and circulation rates on cuttings transport (Akhshik et al., 2015; Bilgesu et al., 2002; Cayeux et al., 2014; Erge and van Oort, 2020; Li et al., 2010; Sun et al., 2014; Zhang et al., 2020). However, most of these CFD studies are only applicable to single-phase fluid flow.

The aforementioned research for multiphase flow have not taken into account the effect of the transient flow pattern transitions that occurs for two-phase flow (gas/liquid) through annular geometries. Effective solids transport in multiphase fluids are highly dependent on the fluid flow pattern (Oyeneyin, 2015) so the flow pattern must be taken into consideration when performing cuttings transport prediction or evaluation. The gas-liquid fluid flow patterns most likely to occur for two-phase flow in an UBD wellbore are the dispersed bubble, bubble, stratified flow and slug flow patterns (Mousavi et al., 2008). Previous experimental and theoretical studies on two-phase flow in either pipes or annuli have shown that the conservation of mass, momentum and energy for two-phase gas-liquid flow are different to that of the single-phase flow and significantly dependent on the prevailing fluid flow pattern (Caetano et al., 1992; Dukler and Hubbard, 1975; Dukler and Taitel, 1986; Mukherjee and Brill, 1985; Taitel and Barnea, 1990; Xiao et al., 1990). Hence, it is required that the wellbore hyraulics and cuttings transport modelling for UBD operations be flow pattern dependent.

In this paper, in order to address the effect of the two-phase gas-liquid flow pattern on the cuttings transport efficiency and wellbore hydraulics for UBD operations, an experimental and theoretical study was conducted. By investigating the effect of both single-phase and two-phase gas-liquid fluid flow on cuttings transport efficiency in the annuli, this research provides key experimental results to characterise the effect of the major drilling parameters that influence hydraulics and cuttings transport in horizontal and inclined wellbores and contributes to the better understanding of the phenomena that take place in cuttings transport in UBD operations. New flow pattern dependent mathematical multi-layered models and several equations were developed to provide a tool that can be applied to evaulate the fluid flow dynamics and cuttings transport efffieciency in the wellbore annuli. The findings of this study can provide a guide to drilling and mud engineers during the design and planning phase of a UBD operation with a method to help facilitate effective hole cleaning during drilling operations.

2.0 Experimental methodology

2.1 Experimental unit

The Multiphase Flow testing facility at the Robert Gordon University, capable of simulating both single-phase and multiphase fluid flow in concentric and eccentric annuli geometries was used to conduct this experimental study. The flow loop consists of transparent test sections that enables the visual observations of the two-phase gas-liquid flow patterns and particle transport mechanism under various experimental conditions. Each annular test section has an outer diameter of 0.1440 m, an inner pipe diameter of 0.0885m which is approximately 2.2 m long. Several test sections can be connected with flanges to achieve a maximum length of about 11 m with roller bearings inserted into the flange areas to allow the inner pipe to rotate smoothly and to allow for the desired concentric or eccentric geometrical position. The schematic diagram of the experimental unit is shown in Fig. 1.

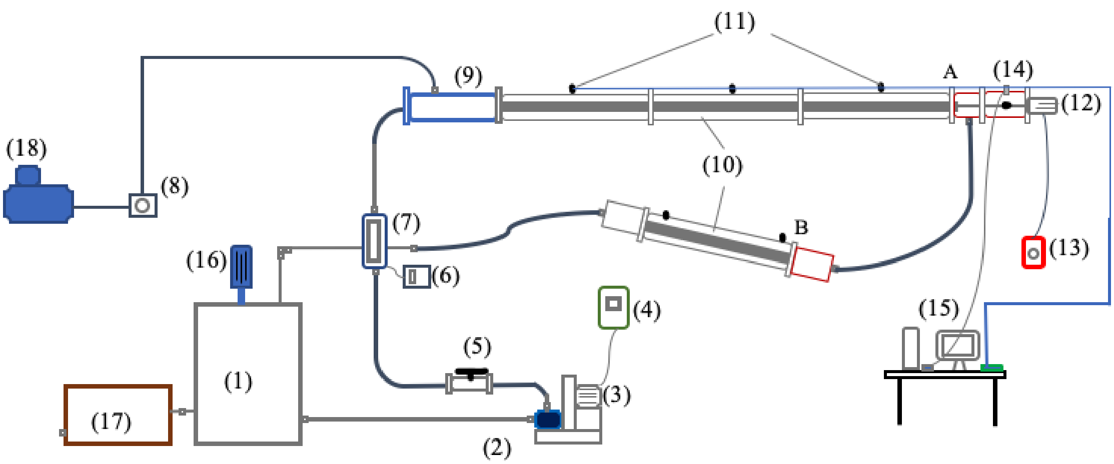

Fig. 1: Schematic diagram of the experimental unit

The experimental rig consists of the following major components: (1) mixing and storage tank; (2) self-priming centrifugal pump; (3) pump motor; (4) frequency inverter for control of the pump motor speed; (5) flow control valve; (6) flowrate indicator; (7) magnetic volumetric flowmeter; (8) air flowrate regulator; (9) steel pipe flow accumulator; (10) transparent annuli test sections; (11) ports for absolute or differential pressure transducers; (12) DC motor responsible for the inner pipe rotation; (13) DC motor speed controller; (14) photoelectric sensor used to determine the real-time inner pipe rotary speed, (15) data acquisition system consisting of a computer and National Instruments devices (NI SCB-68 E series and USB-6009). (16) mechanical agitator; (17) solid particle separation tank designed for the separation of the solid particles from the fluids; and (18) air compressor. While the top and bottom test sections can be setup in both horizontal and inclined orientations, the system is designed in such a way that the DC motor can be transferred from the top to the bottom section at will by interchanging the connections at point A and B (Fig. 1).

2.2 Materials

Water and polymer solutions prepared with a concentration of 0.1% xanthan gum (XG) in water were used in this study to represent the drilling fluid for single-phase experimental tests and as the liquid phase in the air-liquid mixtures for the two-phase flow experimental tests. The XG solutions were prepared by adding XG with a 98% purity to distilled water at a temperature of about 35 ºC under vigorous agitation to ensure that the solute is homogeneously dissolved. After an adequate period of hydration, rheological measurements were carried using a Fann 35SA viscometer to obtain the shear stress to shear rate data of the polymer solutions under ambient conditions (22 ^{0}C). Nonlinear regression was performed on the rheological data, with results showing that the polymer solution was best represented by the Herschel Bulkley rheological model. The rheological parameters obtained for the XG polymer solution are $K = 0.094$, $n = 0.68$, and $\tau_o = 0.001$.

Spherical shaped glass and plastic beads (Fig. 2) were used in this study to represent the cutting particles in order to investigate the efficiency of the cutting transport process in the single-phase and two-phase air-liquid fluid flow in the annuli. A given particle type had a specific colour which provided the benefits of an enhanced visualisation of the cuttings transport dynamics under the various test conditions. The glass and plastic beads used are inert as they do not react with the fluids (water or polymer) and thus, can be recycled.

(a)

(b)

Fig. 2: Image of (a) solids separation tank and (b) glass and plastic beads

Table 1 presents the properties of each of the particle types that were used to represent the cuttings in the experimental tests conducted. In order to obtain specific results for the measured pressure drop and particle transport dynamics for a given particle size and density, some tests were performed using each of the particles alone with the single-phase and two-phase air-liquid fluids. However, other experimental tests were performed with a combination of more than one particle type to investigate the influence of the major drilling parameters and the cuttings transport efficiency.

Table 1: Properties of experimental particles

Particle	Colour	Size, mm	Density, kg/m^3
1	White	1.25	900
2	Transparent	2.00	950
3	Red	4.00	1000
4	Blue	1.65	1500
5	Green	2.40	2000

2.3 Experimental tests

In order to verify the accuracy of the results obtained from the experimental unit, pressure drop measurements were obtained for tests involving the flow of single-phase water in the annuli without inner pipe rotation and favourable results were produced when compared to that which was predicted by the models suggested by Caetano et. al 1992 (Fig.A.1). After verifying the accuracy of the experimental rig, experimental tests were performed in both concentric and eccentric annular geometries using water, polymer, water/air and polymer/air fluids, flowing in horizontal and inclined annuli orientations, with and without inner pipe rotation. The operational ranges for the test conditions considered in this study is presented in Table 2.

Table 2: Operational parameters considered for experiment tests

Parameters	Value range
Eccentricity	0 and 0.7
Rotation	0 to 150 rpm
Angle	0 - 30^0
Air flowrate	0 to 28 m^3/hr
Liquid flowrate	0 to 35 m^3/hr

3.0 Mathematical modelling

The pressure gradient in the wellbore annulus flowing with a two-phase gas-liquid drilling fluid is significantly dependent on the gas-liquid flow pattern and the cuttings transport mechanism. If the drilling fluid velocity is higher than the minimum transport velocity (MTV) for suspension, the cuttings would be transported in the suspension mechanism. However, a stationary bed is formed in the annuli when the drilling fluid velocity is below the MTV required to transport the cuttings in moving bed regime. The stationary bed height increases, thereby increasing the annuli fluid velocity until the point is reached where the oncoming cuttings have enough forces to keep them in suspension or in motion as a moving bed. This reduction in area and the vertical concentration gradient of the cuttings have an impact on the hydraulics of the system. It is assumed that there are three layers that could be formed in the annulus during the drilling operation (Fig. 3): 1) a suspension layer where the cuttings are transported in suspension, 2) a moving bed layer where the cuttings are moving as a bed either on the bottom pipe wall or on top of the stationary bed, and 3) a stationary bed layer. One, two or three of these layers can occur simultaneously in the wellbore annuli depending on the flowing or operating conditions. The critical condition for initiating the cuttings rolling movement may be obtained by defining an average MTV as a function of the major parameters that govern cutting transport, $V_{MR} = f\left(\rho_f, \rho_c, d_c, d_x, \mu_{f,}, g(\rho_c - \rho_f)\right)$. The term $g(\rho_c - \rho_f)$ based on force analysis is the gravitational resistance force acting on the cutting. However, in the inclined annuli, since the force of resistance acting on a cutting is the sum of the component of the gravitational force and the friction force generated between the cutting and the annuli wall in the fluid flow direction, the independent parameter responsible for the effect of the inclination angle and the gravitational force should be modified as $g(\rho_c - \rho_f)[f_s \sin\beta + \cos\beta]$ and $g(\rho_c - \rho_f)\sin\beta$ as the gravitational resistance for cutting suspension (Luo et al., 1992). Thus, the critical condition for the cuttings rolling movement can be expressed as:

$$V_{MR} = f\left(\rho_f, \rho_c, d_c, d_x, \mu_{f,}, g(\rho_c - \rho_f)[f_s \sin\beta + \cos\beta]\right) \qquad \text{(Eq. 1)}$$

The critical condition for the cuttings suspension in the annuli can be expressed as:

$$V_{MS} = f(\rho_f, \rho_c, d_c, d_x, \mu_f, g(\rho_c - \rho_f)\sin\beta) \qquad \text{(Eq. 2)}$$

The MTV for rolling, V_{MR} and suspension, V_{MS} from dimensional analysis may then be expressed respectively as:

$$V_{MR} = M_1 \frac{\mu_f}{d_c \rho_f}\left[\frac{{d_c}^3 \rho_f\, g\, (\rho_c - \rho_f)[\cos\beta + f_s \sin\beta]}{{\mu_f}^2}\right]^{M_2}\left[\frac{d_x}{d_c}\right]^{M_3} \qquad \text{(Eq. 3)}$$

$$V_{MS} = N_1 \frac{\mu_f}{d_c \rho_f}\left[\frac{{d_c}^3 \rho_f\, g\, (\rho_c - \rho_f)\sin\beta}{{\mu_f}^2}\right]^{N_2}\left[\frac{d_x}{d_c}\right]^{N_3} \qquad \text{(Eq. 4)}$$

where M_1, M_2, M_3, N_1, N_2 and N_3 are constants that can be obtained numerically or experimentally.

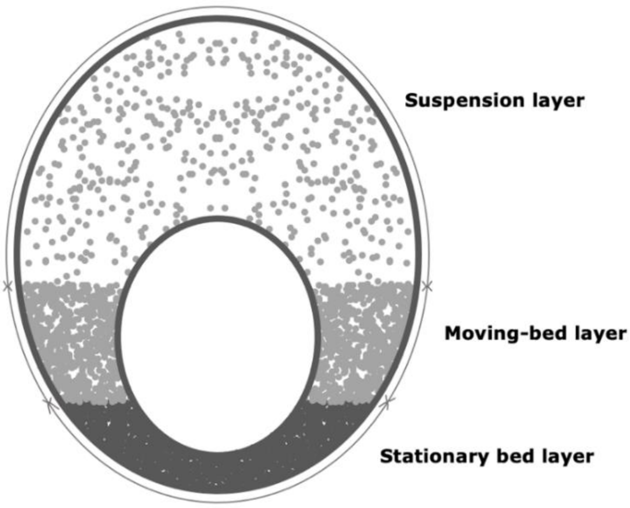

Fig. 3. Configuration of the three-layered cutting transport mechanism in the annuli

The area of the flow through the annuli A_{flow}, can be obtained from the following relationships:

$$Q = A_{flow} V_f \tag{Eq. 5}$$

$$A_{flow} = \frac{Q}{V_f} \tag{Eq. 6}$$

$$V_f = \max(V, V_{MR}) \tag{Eq. 7}$$

$$A_a = A_b + A_{flow} = \frac{\pi\left(d_2{}^2 - d_1{}^2 \right)}{4} \tag{Eq. 8}$$

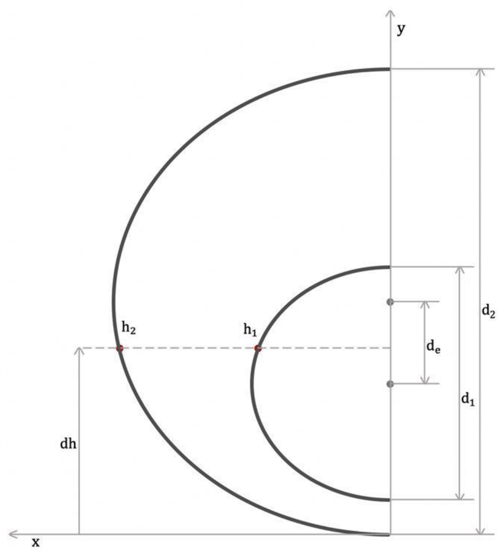

Fig. 4. Annulus geometry schematic for rate of change of bed area with height

From the schematic diagram Fig. 4, the area of the stationary bed in a concentric or eccentric annulus can be obtained by considering the gradient of the area of the bed formed in the annulus. Using geometrical relationships and taking half of the annulus configuration, the rate of change of the bed area may be derived as:

$$\frac{dA_b}{dy} = 2\left[\left(\frac{{d_2}^2}{4} - \left(\frac{d_2}{2}\sin\alpha_2\right)^2\right)^{1/2} - \left(\frac{{d_1}^2}{4} - \left(\frac{d_1}{2}\sin\alpha_1\right)^2\right)^{1/2}\right] \qquad \text{(Eq. 9)}$$

The geometric positions h_2 and h_1 in the Fig. 4 can be expressed respectively as:

$$h_2 = \frac{d_2}{2} + \frac{d_2}{2}\sin\alpha_2 \qquad \text{(Eq. 10)}$$

$$h_1 = \frac{d_2}{2} - d_e + \frac{d_1}{2}\sin\alpha_1 \qquad \text{(Eq. 11)}$$

Where α_1 and α_2 represent the angular position of h_1 and h_2. Since the positions h_2 and h_1 are both equal to the stationary bed height, $h_2 = h_1 = h_b$ the following relationships can be derived:

$$\sin\alpha_2 = \frac{2h_b - d_2}{d_2} \qquad \sin\alpha_1 = \frac{2h_b - d_2 + 2d_e}{d_1} \qquad \text{(Eq. 12)}$$

From the (Eq. 9 to (Eq. 12, the expression for the area of the liquid in a concentric or eccentric annulus can be expressed as:

$$A_b = 2\int_0^{h_b}\left[\left(\frac{{d_2}^2}{4} - \left(\frac{1}{2}(2h_b - d_2)\right)^2\right)^{1/2} - \left(\frac{{d_1}^2}{4} - \left(\frac{1}{2}(2h_b - d_2 + 2d_e)\right)^2\right)^{1/2}\right]dh \qquad \text{(Eq. 13)}$$

The distance between the centre of the outer pipe and the inner pipe d_e can be determined from the following expression:

$$d_e = \frac{1}{2}(d_2 - d_1)e \qquad \text{(Eq. 14)}$$

(Eq. 13 can be solved analytically to yield the following rigorous equations for the area of the stationary bed in a concentric or eccentric annulus:

$$X1(h_b) = \frac{{d_2}^2}{4}\sin^{-1}\left(\frac{2h_b - d_2}{d_2}\right) - \frac{{d_1}^2}{4}\sin^{-1}\left(\frac{2h_b - d_2 + 2d_e}{d_1}\right) \qquad \text{(Eq. 15)}$$

$$X2(h_b) = \frac{1}{2}\left((2h_b - d_2)\left(h_b d_2 - {h_b}^2\right)^{1/2} + (d_2 - 2d_e - 2h_b)\left[\begin{matrix}(d_2 - 2d_e)h_b - {h_b}^2 \\ +\frac{1}{4}5{d_1}^2 - \left(\frac{1}{2}(d_2 - 2d_e)\right)^2\end{matrix}\right]^{1/2} + \frac{1}{4}\pi {d_2}^2\right) \qquad \text{(Eq. 16)}$$

$$X3(h_b) = \frac{1}{2}(d_2 - 2d_e)\left(\frac{1}{4}{d_1}^2 - \left(\frac{1}{2}(d_2 - 2d_e)\right)^2\right)^{1/2} + \frac{1}{4}{d_1}^2\sin^{-1}\left(\frac{d_2 - 2d_e}{d_1}\right) \qquad \text{(Eq. 17)}$$

The area of the stationary bed in a concentric or eccentric annulus can hereby be obtained from the summation of the (Eq. 15 to (Eq. 17 yields:

$$A_b = X1(h_b) + X2(h_b) + X3(h_b) \quad \text{(Eq. 18)}$$

In this mathematical model development, the multiphase gas-liquid flow pattern is taken into consideration with the cuttings transport mechanism, making this a major improvement from the previously developed multi-layered models. The mass, momentum and energy conservations for multiphase flowing fluids in conduits are flow pattern dependent therefore, the model development using the governing conservation equations need to be flow pattern specific. The model development is based on the assumption that the drilling activity is carried out at operating conditions where the suspension, moving bed and stationary bed layers may be formed individually or simultaneously in the annulus. The cutting particles would be transported in homogeneous suspension if $V_f > V_{MS}$, $h_b = 0$, and a suspension and moving bed layer would be formed if $V_f < V_{MS}$, $V_f > V_{MR}$, $h_b = 0$. However, if $V_f < V_{MR}$, a stationary bed is formed ($h_b > 0$) and increases until $V_f = V_{MR}$. Thus, the flow area in the annuli is reduced and the oncoming particles forms a suspension and moving bed layer above the stationary bed layer. As highlighted in the literature, for UBD operations, the gas-liquid fluid flow patterns most likely to exist in the wellbore are the dispersed bubble, bubble, stratified flow and slug flow pattern. Thus, in this study these are the fluid flow patterns that were considered in the model development.

3.1 Bubble and dispersed bubble flow

Assuming that the flow is steady-state and there is no slip between the cuttings and fluid phase, the continuity equation for the cuttings and the fluid phase in a given control volume may be written as:

Cuttings phase:

$$\frac{\partial(\rho_c C_1 A_1 V_1)}{\partial L} + \frac{\partial(\rho_c C_2 A_2 V_2)}{\partial L} + \frac{\partial(\rho_c C_3 A_3 V_3)}{\partial L} = 0 \quad \text{(Eq. 19)}$$

Drilling fluid phase:

$$\frac{\partial(\rho_f(1 - C_1)A_1 V_1)}{\partial L} + \frac{\partial(\rho_f(1 - C_2)A_2 V_2)}{\partial L} + \frac{\partial(\rho_f(1 - C_3)A_3 V_3)}{\partial L} = 0 \quad \text{(Eq. 20)}$$

Integrating the continuity equations across the control volume, and acknowledging that the stationary bed is not moving $V_3 = 0$, the mass balance of the cuttings and the fluid phase can then be expressed as:

Cuttings phase:

$$\rho_c C_1 A_1 V_1 + \rho_c C_2 A_2 V_2 = \rho_c C_c A_a V_a \quad \text{(Eq. 21)}$$

Drilling fluid phase:

$$\rho_m (1 - C_1)A_1 V_1 + \rho_m (1 - C_2)A_2 V_2 = \rho_m (1 - C_c)A_a V_a \quad \text{(Eq. 22)}$$

where C_c, is the input cuttings concentration.

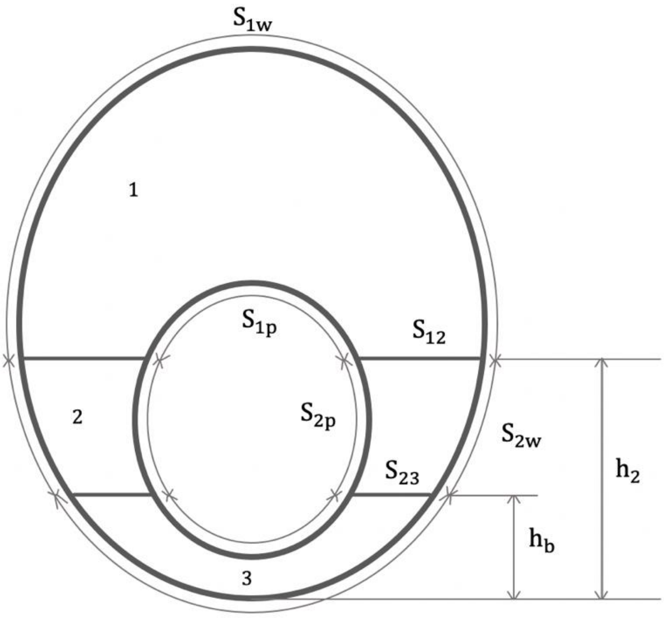

Fig. 5. Schematic diagram of the three-layer model for dispersed bubble flow

The momentum equations for the dispersed bubble flow can be obtained by considering the sum of the forces acting on each of the layers (Fig. 5):

Suspension layer:

$$-\frac{dP}{\partial L}+\frac{\tau_{1w}S_{1w}}{A_1}+\frac{\tau_{1p}S_{1p}}{A_1}-\frac{\tau_{12}S_{12}}{A_1}+\rho_1 g\sin\theta=0 \quad \text{(Eq. 23)}$$

Moving bed layer:

$$-\frac{dP}{\partial L}+\frac{\tau_{2w}S_{2w}}{A_2}+\frac{\tau_{2p}S_{2p}}{A_2}+\frac{\tau_{12}S_{12}}{A_2}+\frac{\tau_{23}S_{23}}{A_2}+\rho_2 g\sin\theta=0 \quad \text{(Eq. 24)}$$

The mixture density for each of the layers are given as:

$$\rho_1=\rho_m(1-C_1)+\rho_c C_1 \quad \text{(Eq. 25)}$$

$$\rho_2=\rho_m(1-C_1)+\rho_c C_2 \quad \text{(Eq. 26)}$$

where ρ_m, defined by the (Eq. 26, is the gas-liquid mixture density.

$$\rho_m=\rho_L\lambda_L+\rho_G(1-\lambda_L) \quad \text{(Eq. 27)}$$

The wetted perimeters required for the solution of these equations are dependent on the height of the stationary bed h_b and the height of the suspension-moving bed interface h_2 as shown in the Fig. 5. The functions for the wetted perimeters for each of the flow patterns were derived solely from wellbore geometry and trigonometry and are presented in the Appendix C. The cross-sectional area of each of the layers can be computed using the (Eq. 15 to (Eq. 18 as a function of the interfacial heights h_2 and h_b:

$$A_1=A_a-\left(X1(h_2)+X2(h_2)+X3(h_2)\right) \quad \text{(Eq. 28)}$$

$$A_b = X1(h_b) + X2(h_b) + X3(h_b) \quad \text{(Eq. 29)}$$

$$A_2 = A_a - A_1 - A_b \quad \text{(Eq. 30)}$$

If a stationary bed does not exist, and only a moving bed and suspension layer is present in the annuli, it is important to note that the interface parameter S_{23} becomes zero and S_{1p}, S_{2p}, S_{12}, S_{1w}, and S_{2w} all have non-zero values. However, if only a suspension mechanism exists in the annuli, only the parameter S_{1w} exists and thus, $S_{1w} = \pi d_2$.

3.2 Stratified flow

The vertical cuttings concentration in stratified flow pattern is different to that which is experienced by the dispersed bubble flow pattern. When the stratified gas-liquid flow is formed in the wellbore annuli, the cuttings would fall to the liquid phase flowing below the gas phase due to density differences. This leads to the formation of four distinctive layers in the annuli where the suspension and moving bed layers are embedded in the liquid phase alone (Fig. 6). The layer one only contains all of the gas phase, hence the velocity of layer 1 can be expressed as a function of the input gas flowrate into the wellbore from:

$$V_1 = \frac{Q_G}{A_1} \quad \text{(Eq. 31)}$$

Since there are no cuttings traveling in the gas phase in layer 1, the material balance for the cuttings and the liquid phase in layers 2 and 3 may be expressed as:

Cuttings phase:

$$\rho_c C_2 A_2 V_2 + \rho_c C_3 A_3 V_3 = \rho_c C_c Q_L \quad \text{(Eq. 32)}$$

Drilling fluid phase:

$$\rho_L (1 - C_2) A_2 V_2 + \rho_L (1 - C_3) A_3 V_3 = \rho_L (1 - C_c) Q_L \quad \text{(Eq. 33)}$$

In some cases, the cuttings in the liquid phase of the stratified flow travels as a moving bed as the liquid velocity is not high enough to suspend the particles. Thus, only a moving bed and stationery bed may exist in the annuli and in such cases $C_2 = 0$.

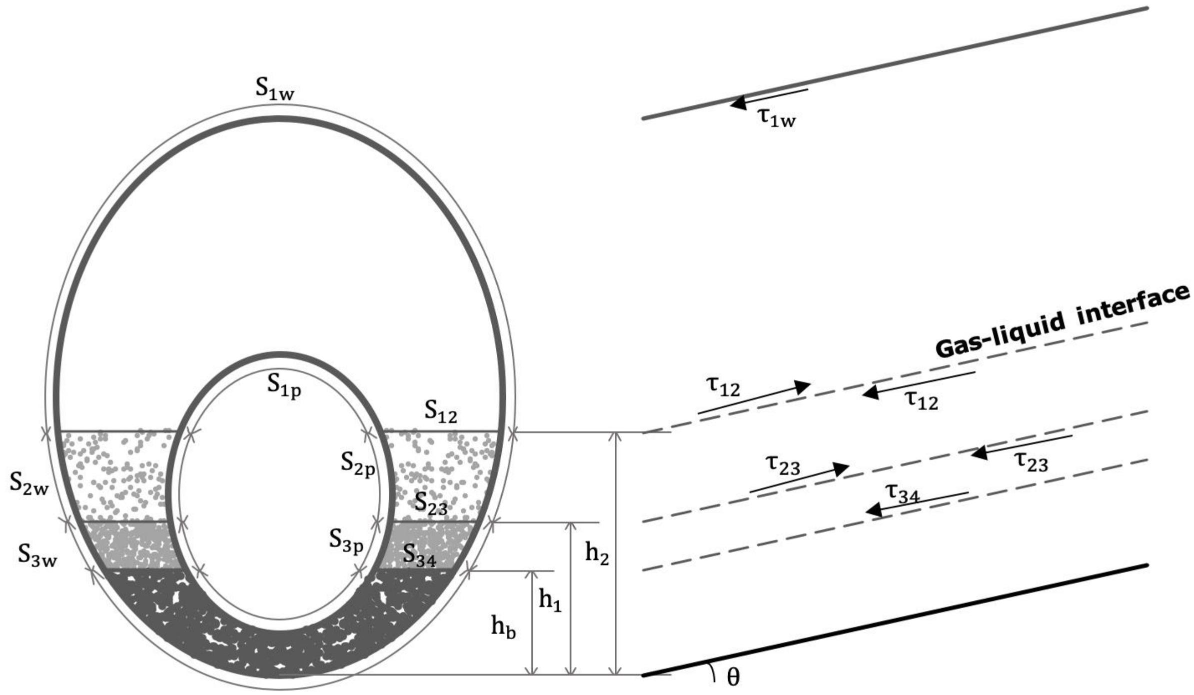

Fig. 6. Schematic diagram of the four-layer model for stratified (gas, liquid and cuttings) flow

The momentum equations obtained from considering the sum of the forces acting on each of the layers may be expressed as:

Layer 1: Gas phase

$$-\frac{dP}{\partial L}+\frac{\tau_{1w}S_{1w}}{A_1}+\frac{\tau_{1p}S_{1p}}{A_1}-\frac{\tau_{12}S_{12}}{A_1}+\rho_1 g\sin\theta=0 \quad \text{(Eq. 34)}$$

Layer 2: Suspension layer (liquid phase)

$$-\frac{dP}{\partial L}+\frac{\tau_{2w}S_{2w}}{A_2}+\frac{\tau_{2p}S_{2p}}{A_2}+\frac{\tau_{12}S_{12}}{A_2}-\frac{\tau_{23}S_{23}}{A_2}+\rho_2 g\sin\theta=0 \quad \text{(Eq. 35)}$$

Layer 3: Moving bed layer (liquid phase)

$$-\frac{dP}{\partial L}+\frac{\tau_{3w}S_{3w}}{A_3}+\frac{\tau_{3p}S_{3p}}{A_3}+\frac{\tau_{23}S_{23}}{A_3}+\frac{\tau_{34}S_{34}}{A_3}+\rho_3 g\sin\theta=0 \quad \text{(Eq. 36)}$$

The density of layer 1 is the density of the gas phase as only the gas phase is flowing in this layer. Thus, the in-situ density for each of the layers are given as:

$$\rho_1=\rho_G \quad \text{(Eq. 37)}$$

$$\rho_2=\rho_L(1-C_2)+\rho_c C_2 \quad \text{(Eq. 38)}$$

$$\rho_3 = \rho_L(1 - C_3) + \rho_c C_3 \quad \text{(Eq. 39)}$$

The wetted perimeters required for the solution of the stratified flow momentum equations are not only dependent on the height of the stationary bed h_b and the height of the suspension-moving bed interface h_1, but is dependent on the height of the gas-liquid interface h_2. The cross-sectional area of each of the layers can be computed using a similar approach to that which was used in the dispersed bubble flow pattern. The functions required for determining the area of the layers may be expressed as:

$$A_1 = A_a - \left(X1(h_2) + X2(h_2) + X3(h_2)\right) \quad \text{(Eq. 40)}$$

$$A_b = X1(h_b) + X2(h_b) + X3(h_b) \quad \text{(Eq. 41)}$$

$$A_3 = \left(X1(h_1) + X2(h_1) + X3(h_1)\right) - A_b \quad \text{(Eq. 42)}$$

$$A_2 = A_a - A_1 - A_3 - A_b \quad \text{(Eq. 43)}$$

The wall and interfacial shear stresses in the mathematical models can be determined respectively from the following equations:

$$\tau_i = \frac{f_i \rho_i V_i^2}{2} \quad \text{(Eq. 44)}$$

$$\tau_{ij} = \frac{f_i \rho_i \left(V_i - V_j\right)^2}{2} \quad \text{(Eq. 45)}$$

where subscripts i and j indicate the position of the layers in the annulus. The equations required to calculate the wall and interfacial friction factors and shear stresses are given in the Appendix B and C.

3.3 Slug flow

The cutting transport modelling for the slug flow pattern is relatively more complex than that of the other flow patterns. This is because there is not only the formation of several vertical layers due to the disparities in the cutting transport mechanism, but there exist two separate regions in the axial direction, where the phase configuration and the fluid shearing forces differ significantly. A fully developed slug unit is composed of the axial movement of a slug body accompanied by a liquid-film/gas pocket region. In the slug unit, if the drilling fluid annuli velocity in the slug body is below the MTV required to keep the cuttings mobile, this would lead to the formation of a stationary cuttings bed and the flow of the oncoming liquid-film/gas pocket region over the stationary bed. Slug flow has a complex and highly transient hydrodynamic behaviour making predictions difficult because of its unsteady nature and the fluid forces or conservation of momentum within the slug body differing from those within the liquid-film/gas pocket region.

The fundamental idea presented by Taitel and Barnea (1990) to predict pressure drop across a slug unit in a horizontal and upward inclined pipe flow have been adopted and modified to develop mechanistic models for the evaluation of cuttings transport and pressure gradient for a fully developed slug flow with cuttings in the concentric and eccentric annuli. Fig 7 shows the gas-liquid configuration and the different cuttings transport mechanisms that may exist in a fully developed slug flow in an inclined annulus.

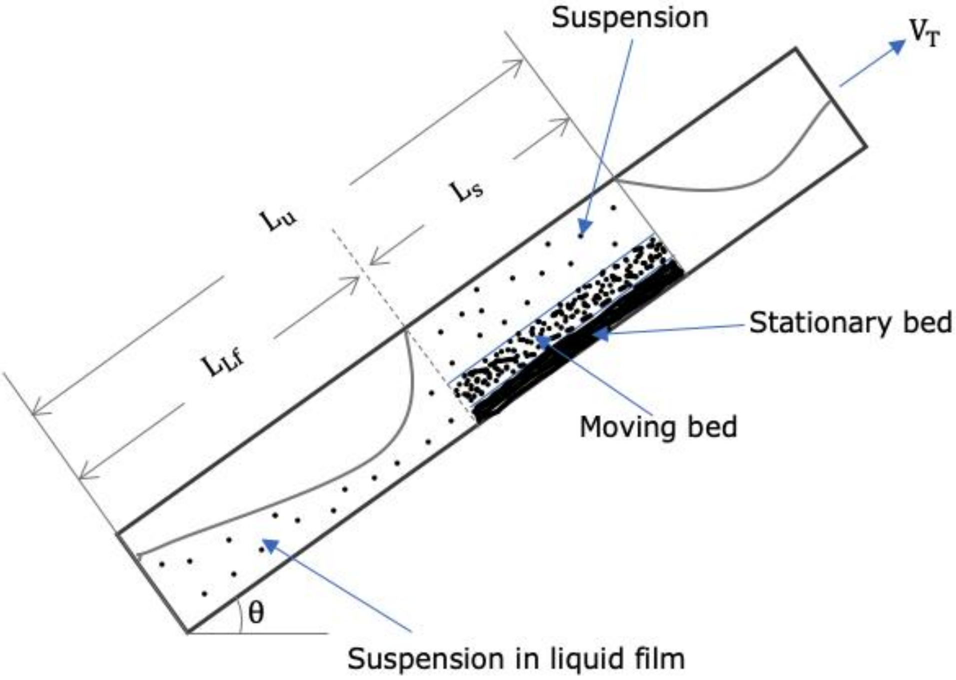

Fig. 7. Fully developed slug flow with cuttings in an inclined wellbore annulus

The liquid and gas flowrates in a control volume containing the liquid slug and liquid-film/gas pocket region can be expressed respectively as:

$$Q_L = V_{Ls}A_{Ls} + V_{Lf}A_{Lf} \quad \text{(Eq. 46)}$$

$$Q_G = V_{Gs}A_{Gs} + V_{Gf}A_{Gf} \quad \text{(Eq. 47)}$$

The time taken for the slug unit t_u, the liquid slug region t_s, and the liquid-film/gas pocket region t_{Lf}, to cross a given point in the wellbore annulus can be expressed in terms of the translational velocity, V_T:

$$t_u = \frac{L_u}{V_T} \qquad t_s = \frac{L_s}{V_T} \qquad t_{Lf} = \frac{L_{Lf}}{V_T} \quad \text{(Eq. 48)}$$

where the length of a fully developed slug unit is given by: $L_u = L_s + L_{Lf}$

From (Eq. 46 to (Eq. 48 the liquid volume in the slug unit can be expressed as:

$$Q_L t_u = V_{Ls}A_{Ls}t_s + V_{Lf}A_{Lf}t_{Lf} \quad \text{(Eq. 49)}$$

$$Q_L - V_{Ls}A_{Ls}\frac{L_s}{L_u} - V_{Lf}A_{Lf}\frac{L_{Lf}}{L_u} = 0 \quad \text{(Eq. 50)}$$

Considering that the liquid level is not constant throughout the length of the liquid-film/gas pocket region, (Eq. 50 can be written as:

$$Q_L - V_{Ls}A_{flow}H_{Ls}\frac{L_s}{L_u} - \int_0^{L_{Lf}} \frac{V_{Lf}A_{flow}H_{Lf}}{L_u}\,\partial L_{Lf} = 0 \quad \text{(Eq. 51)}$$

The liquid film velocity can be obtained from the mass balance due to the pickup rate of the liquid film in the front of the slug as follows:

$$(V_T - V_{Ls})H_{Ls} = (V_T - V_{Lf})H_{Lf} \quad \text{(Eq. 52)}$$

$$V_{Lf} = V_T - \frac{(V_T - V_{Ls})H_{Ls}}{H_{Lf}} \quad \text{(Eq. 53)}$$

Thus, the liquid mass balance relationship over the entire slug unit may be expressed as follows:

$$Q_L - V_{Ls}A_{flow}H_{Ls}\frac{L_s}{L_u} - \int_0^{L_{Lf}} \left(V_T - \frac{(V_T - V_{Ls})H_{Ls}}{H_{Lf}}\right)\frac{A_{flow}H_{Lf}}{L_u}\,\partial L_{Lf} = 0 \quad \text{(Eq. 54)}$$

$$Q_L - V_{Ls}A_{flow}H_{Ls} + \frac{V_T A_a H_{Ls} L_{Lf}}{L_u} - \frac{V_T A_{flow}}{L_u}\int_0^{L_{Lf}} H_{Lf}\,\partial L_{Lf} = 0 \quad \text{(Eq. 55)}$$

The material balance of the cuttings and fluid phase in the entire fully developed slug unit may be expressed as:

Cuttings phase:

$$\rho_c C_1 A_1 V_1 L_s + \rho_c C_2 A_2 V_2 L_s + \rho_c C_{Lf} A_{flow}\int_0^{L_{Lf}} V_{Lf} H_{Lf}\,\partial L_{Lf} = \rho_c C_c A_a V_a L_u \quad \text{(Eq. 56)}$$

Drilling fluid phase:

$$\rho_s (1 - C_1) A_1 V_1 L_s + \rho_s (1 - C_2) A_2 V_2 L_s +$$

$$\rho_L (1 - C_{Lf}) A_{flow}\int_0^{L_{Lf}} V_{Lf} H_{Lf}\,\partial L_{Lf} + \rho_G A_{flow}\int_0^{L_{Lf}} V_{Gf}(1 - H_{Lf})\,\partial L_{Lf} = \rho_m (1 - C_c) A_a V_a L_u \quad \text{(Eq. 57)}$$

3.3.1 Slug body region

The mass and momentum balance equations in the slug body region of the fully developed slug unit are similar to that of the dispersed bubble flow. In the slug body region, the cuttings can be both or either in suspension or mobile as a moving bed. The momentum equations for the suspension and moving-bed layer may be expressed as:

Suspension layer:

$$-\left.\frac{\partial P}{\partial L}\right)_s + \frac{\tau_{1w}S_{1w}}{A_1} + \frac{\tau_{1p}S_{1p}}{A_1} - \frac{\tau_{12}S_{12}}{A_1} + \rho_1 g \sin\theta = 0 \quad \text{(Eq. 58)}$$

Moving bed layer:

$$-\left.\frac{\partial P}{\partial L}\right)_s + \frac{\tau_{2w}S_{2w}}{A_2} + \frac{\tau_{2p}S_{2p}}{A_2} + \frac{\tau_{12}S_{12}}{A_2} + \frac{\tau_{23}S_{23}}{A_2} + \rho_2 g \sin\theta = 0 \quad \text{(Eq. 59)}$$

The mixture density for each of the layers are given as:

$$\rho_1 = \rho_s(1 - C_1) + \rho_c C_1 \qquad \text{(Eq. 60)}$$

$$\rho_2 = \rho_s(1 - C_2) + \rho_c C_2 \qquad \text{(Eq. 61)}$$

The fluid density in the slug body ρ_s is obtained as a function of the liquid hold up in the slug body H_{Ls} and not the input or no-slip liquid hold.

$$\rho_s = \rho_L H_{Ls} + \rho_G(1 - H_{Ls}) \qquad \text{(Eq. 62)}$$

3.3.2 Liquid-film/gas pocket region

The faster flowing slug body moving behind the slower liquid film overruns and picks up the liquid in the liquid film and accelerates it to the slug velocity. The acceleration of the liquid film is accompanied with a change in the height of the liquid film, the liquid hold-up, the velocity of the liquid film and the interfacial and wall shear stresses in the axial direction of the flow. It is assumed that the cuttings flowing in the liquid-film/gas pocket region are only located in the liquid film due to density differences, so the cuttings benefit from the acceleration of the liquid film, keeping them in the suspension mechanism. Fig. 8 shows the geometric configuration of the liquid film/gas pocket region which contains the gas layer on top, a liquid region with cuttings suspension and stationary bed.

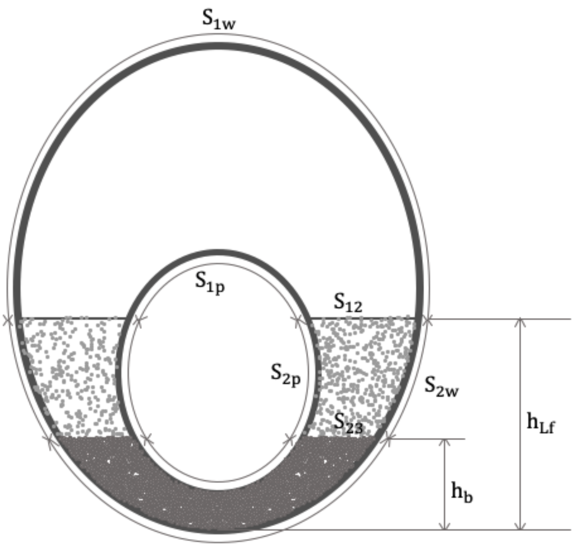

Fig. 8. Schematic diagram of the mathematical model for liquid film/gas pocket region

The liquid film hydrodynamics analysis in the translational velocity co-ordinate system permits the respective expression of the conservation of momentum equations for the gas pocket and the liquid film in the drilling annulus as:

Layer 1: Gas pocket

$$-\frac{\partial P}{\partial L} + \rho_G v_{Gf}\frac{\partial v_{Gf}}{\partial L} + \frac{\tau_{1w}S_{1w}}{A_{Gf}} + \frac{\tau_{1p}S_{1p}}{A_{Gf}} + \frac{\tau_{12}S_{12}}{A_{Gf}} + \rho_G g\sin\theta - \rho_G g\cos\theta\frac{\partial h_{Lf}}{\partial L} = 0 \qquad \text{(Eq. 63)}$$

Layer 2: Liquid film and drilled cuttings

$$-\frac{\partial P}{\partial L} + \rho_{Lfc} v_{Lf} \frac{\partial v_{Lf}}{\partial L} + \frac{\tau_{2w} S_{2w}}{A_{Lf}} + \frac{\tau_{2p} S_{2p}}{A_{Lf}} - \frac{\tau_{12} S_{12}}{A_{Lf}} + \frac{\tau_{23} S_{23}}{A_{Lf}} + \rho_{Lfc} g \sin\theta - \rho_{Lfc} g \cos\theta \frac{\partial h_{Lf}}{\partial L} = 0 \quad \text{(Eq. 64)}$$

where ρ_{Lfc}, is the mixture density of the liquid and the cuttings in the liquid film, given as:

$$\rho_{Lfc} = \rho_L (1 - C_{Lf}) + \rho_c C_{Lf} \quad \text{(Eq. 65)}$$

The relative velocities of the liquid film and gas are given as:

$$v_{Lf} = V_T - V_{Lf} \text{ and } v_{Gf} = V_T - V_{Gf} \quad \text{(Eq. 66)}$$

Using the (Eq. 52 and(Eq. 53, the relative velocity of the liquid film can be expressed as:

$$v_{Lf} = \frac{(V_T - V_{Ls}) H_{Ls}}{H_{Lf}} \quad \text{(Eq. 67)}$$

Similarly, from the mass balance of the gas phase in the liquid-film/gas pocket region, the relative velocity of the gas may then be expressed as follows:

$$(V_T - V_{Gs})(1 - H_{Ls}) = (V_T - V_{Gf})(1 - H_{Lf}) \quad \text{(Eq. 68)}$$

$$v_{Gf} = \frac{(V_T - V_{Gs})(1 - H_{Ls})}{(1 - H_{Lf})} \quad \text{(Eq. 69)}$$

The change in the relative velocities with length is a function of the hold-up of the liquid film and can be expressed as:

$$\frac{\partial v_{Lf}}{\partial L} = \frac{\partial v_{Lf}}{\partial H_{Lf}} \times \frac{\partial H_{Lf}}{\partial h_{Lf}} \times \frac{\partial h_{Lf}}{\partial L} \quad \text{(Eq. 70)}$$

$$\frac{\partial v_{Gf}}{\partial L} = \frac{v_{Gf}}{\partial H_{Lf}} \times \frac{\partial H_{Lf}}{\partial h_{Lf}} \times \frac{\partial h_{Lf}}{\partial L} \quad \text{(Eq. 71)}$$

$$\frac{\partial v_{Lf}}{\partial H_{Lf}} = \frac{(V_T - V_{Ls}) H_{Ls}}{H_{Lf}^2} \quad \text{(Eq. 72)}$$

$$\frac{\partial v_{Gf}}{\partial H_{Lf}} = \frac{(V_T - V_{Gs})(1 - H_{Ls})}{(1 - H_{Lf})^2} \quad \text{(Eq. 73)}$$

The shear stresses in (Eq. 63 and (Eq. 64 should be calculated using the actual velocity of the fluids rather than the relative velocities. The equations for the shear stresses in the liquid film is presented in the Appendix C. Substituting (Eq. 63 into (Eq. 64to eliminate the pressure gradient term, an ordinary differential equation for the change in the liquid film height in the axial direction can be obtained:

$$\frac{\partial h_{Lf}}{\partial L} = \frac{\frac{\tau_{2w} S_{2w}}{A_{Lf}} + \frac{\tau_{2p} S_{2p}}{A_{Lf}} - \frac{\tau_{1w} S_{1w}}{A_{Gf}} - \frac{\tau_{1p} S_{1p}}{A_{Gf}} + \frac{\tau_{23} S_{23}}{A_{Lf}} - \tau_{12} S_{12} \left(\frac{1}{A_{Lf}} + \frac{1}{A_{Gf}}\right) + (\rho_{Lfc} - \rho_G) g \sin\theta}{\rho_G v_{Gf} \frac{(V_T - V_{Gs})(1 - H_{Ls})}{(1 - H_{Lf})^2} \frac{\partial H_{Lf}}{\partial h_{Lf}} - \rho_{Lfc} v_{Lf} \frac{(V_T - V_{Ls}) H_{Ls}}{H_{Lf}^2} \frac{\partial H_{Lf}}{\partial h_{Lf}} + (\rho_{Lfc} - \rho_G) g \cos\theta} \quad \text{(Eq. 74)}$$

$$\frac{\partial H_{Lf}}{\partial h_{Lf}} = 2\frac{\left[\left(\frac{d_2{}^2}{4} - \left(\frac{1}{2}(2h_b - d_2)\right)^2\right)^{1/2} - \left(\frac{d_1{}^2}{4} - \left(\frac{1}{2}(2h_b - d_2 + 2d_e)\right)^2\right)^{1/2}\right]}{A_{flow}} \quad \text{(Eq. 75)}$$

(Eq. 74 has to be integrated numerically to yield the liquid film profile $h_{Lf}(L)$, and also to determine the liquid holdup and liquid film velocity distributions. The boundary condition for integrating the first-order differential equation is $h_{Lf}(L = 0) = h_{Lf0}$ corresponding to $v_{Lf}(L = 0) = V_T - V_{Ls}$. Before starting the numerical integration, the boundary condition is obtained by first solving the (Eq. 76 to obtain h_{Lf0}

$$f(h_{Lf0}) = H_{Ls} - \frac{X1(h_{Lf0}) + X2(h_{Lf0}) + X3(h_{Lf0}) - A_b}{A_{flow}} \quad \text{(Eq. 76)}$$

The numerical integration of the differential equation is performed while checking that (Eq. 55 is satisfied. Once the mass balance is satisfied, the integration stops and yields the length of the liquid film in the liquid-film/gas pocket region L_{Lf}. The total annuli pressure drop experienced by the flow can be obtained from the global force and momentum balance across the entire slug unit. The global pressure drop across a slug unit is written as the summation of the pressure drop in the slug body region and the pressure drop in the liquid film region. The average density of the cuttings-fluid mixture in the liquid-film/gas pocket region can be determined from the flowing equation:

$$\rho_{LfA} = \frac{\rho_{Lfc}}{L_{Lf}}\int_0^{L_{Lf}} H_{Lf}\ \partial L_{Lf} + \frac{\rho_G}{L_{Lf}}\int_0^{L_{Lf}} (1 - H_{Lf})\ \partial L_{Lf} \quad \text{(Eq. 77)}$$

Thus, the total pressure drop across the entire slug unit and annuli pressure gradient can be expressed respectively as:

$$\Delta P_u = \left.\frac{dP}{\partial L}\right)_s L_s + \rho_{LfA} g \sin\theta\, L_{Lf} + \int_0^{L_{Lf}} \frac{\tau_{2w}S_{2w} + \tau_{2p}S_{2p} + \tau_{1w}S_{1w} + \tau_{1p}S_{1p} + \tau_{23}S_{23}}{A_a - A_b}\, dL \quad \text{(Eq. 78)}$$

$$\frac{dP}{dL} = \frac{\Delta P_u}{L_u} \quad \text{(Eq. 79)}$$

The mechanism at which the cutting particles are dispersed in the suspension layer can be described by the diffusion equation:

$$\epsilon_c \frac{d^2C}{dy^2} + v_t \frac{dC}{dy} = 0 \quad \text{(Eq. 80)}$$

From the integration of (Eq. 80, the concentration profile of the suspension layer existing in the dispersed bubble, bubble, stratified and the slug body region of the slug flow pattern can be expressed as:

$$C(y) = C_{Mb} \exp\left(-\frac{\epsilon_c (y - h_2)}{v_t}\right) \quad \text{(Eq. 81)}$$

The cutting concentration of the moving bed layer, C_{Mb} is assumed to be 0.52 due to cubic packing (Doron and Barnea, 1993). Before the application of the flow pattern dependent multi-layered model, the prediction of the fluid flow pattern may be required. However, the gas-liquid fluid flow pattern prediction can be performed using the methods suggested in literature (Caetano et al., 1992; Ibarra et al., 2019). It is important to note that the mathematical models are only valid for horizontal and inclined flows and does not taken into account the effect of the inner pipe rotation. The closure and geometric relationships required for each of the flow patterns and the procedure for the solution of the mathematical models are presented in Appendix B, C and D.

4.0 Results and discussion

The effect of some of the major parameters on cuttings transport were analysed and the mathematical model predictions were compared to the experimental results for the different flow patterns. Fig. A.2 shows examples of the cuttings transport mechanisms occurring in different flow patterns for some of the experimental tests that were conducted in this study. These along with Fig. 9 show that in the stratified and slug fluid flow patterns, the solid particles are transported only in the liquid-phase as there are no particles present in the gas-phase for both the Newtonian and non-Newtonian fluids. This justifies the assumption that was made towards the development of the mathematical models for the stratified and slug flow patterns. The experimental study carried out for both single-phase and two-phase flow in the annuli show that the effect of the drilling parameters on hole cleaning for two-phase flow is highly dependent on the prevailing gas-liquid fluid flow pattern and may differ from that of the single-phase flow. In general, for the flow patterns investigated in this study, the dispersed bubble flow pattern was found to be more effective for hole cleaning while the stratified flow pattern was the worst for cutting transport. To optimise UBD operations, effective cutting transport must be achieved. Thus, it is important to understand and consider the effects of the gas-liquid fluid flow pattern variations that may occur during UBD operations and the influence of these flow patterns on the major drilling parameters. In order to analyse the effect of the flow pattern on some of the major drilling parameters, experimental tests performed under two-phase gas-liquid flow conditions with or without solid particles were compared to those that were obtained under single-phase flow conditions for both Newtonian and non-Newtonian flow mixtures:

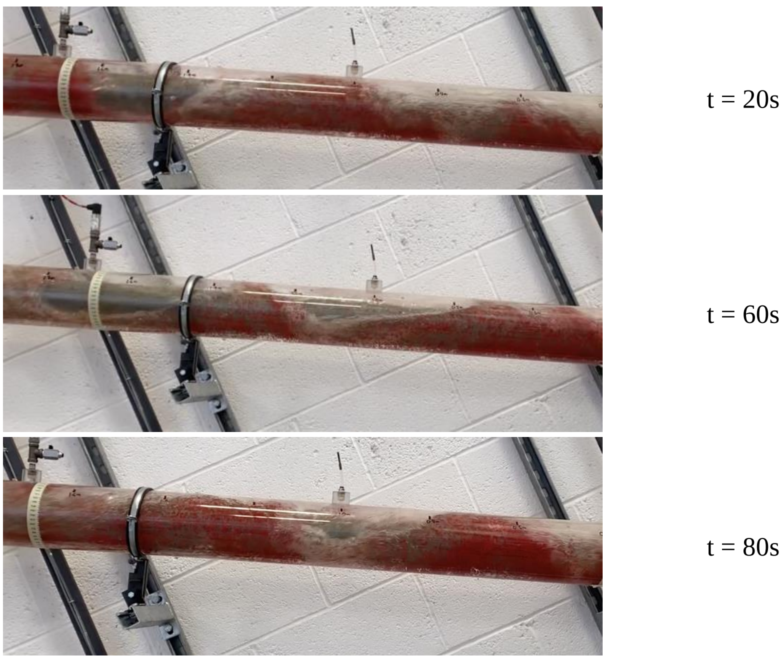

Fig. 9. Particle transport dynamics with time in the slug flow pattern

4.1 Fluid flowrate

The air-liquid fluid flow pattern generated in the annuli for all the experimental tests were strictly dependent on the air and liquid flowrates and were not influenced by the introduction of solid particles. The air-liquid fluid flow pattern formed in the concentric and eccentric annuli was independent of the cuttings concentration for experiments that were performed with various volumetric concentrations of up to 10%. The experimental tests showed that the fluid circulation rate must be high enough to ensure that the particles are transported above the MTV required to at least slide or drag the particles along the bottom of the annuli. However, for a gas-liquid fluid flow, this circulation rate is highly dependent on the fluid flow pattern. For instance, in Fig.A.3 the single-phase fluid flowing at a flowrate of about 30 m^3/hr had the cuttings sliding along the bottom of the annuli creating the moving bed transport mechanism, but the two-phase fluids formed a stationary bed at relatively higher mixture flowrates. The stratified and slug flow patterns formed a stationary bed in the annuli at gas-liquid mixture flowrates of about 35 m^3/hr and 42 m^3/hr respectively. Thus, for UBD operations, the flow pattern must be considered along with the gas-liquid flowrates in order to optimise hole cleaning. However, it should be noted that the type of the fluid flow pattern formed in the annuli is also a function of the gas-liquid in-situ flowrates.

4.2 Inclination Angle

The particle movement in the annuli is highly dependent on the wellbore inclination angle. However, the effect of the wellbore inclination angle on the transport of particles is not independent of the drilling fluid flow pattern. Unlike the single-phase flow, the flow configuration or fluid distribution of two-phase flow in the annuli is affected by the inclination angle of the flow and in some cases if the gas-liquid flowrate is constant, an increase in pipe angle may change the gas-liquid flow pattern from one form to another. This angle effect on the fluid distribution or gas-liquid flow pattern is an additional effect that influences the annuli hydraulics and particle transport efficiency for two-phase flow. Fig.A.4 shows an example of a scenario where gas flowrate of 24 m^3/hr and a liquid flowrate of 21 m^3/hr is passed simultaneously into a horizontal and 20^o inclined annuli test sections thereby generating the slug flow pattern without the presence of particles. It can be seen that the gas-liquid distribution of the flow in the horizontal annuli differs significantly from that of the inclined annuli even though the slug flow pattern exists in both cases. Experimental tests showed that while the horizontal case had a longer liquid film length, the liquid film length decreased with an increase in the inclination angle and the local mixture properties of the fluid was also influenced by the inclination angle (Fig.A.4). The change in the liquid film length with the inclination angle can be predicted from the solution of the slug flow multi-layered model. Fig. 10 and Fig. 11 presents some of the experimental results for the effect of the wellbore inclination angle on the cuttings transport efficiency in the concentric and eccentric annuli. Experimental measurements of the minimum transport velocity, MTV were obtained by introducing the particles of a given concentration into the flow and recording the flowrate at which the particles are fully suspended or rolling at the bottom of the annuli and just below which a stationary bed is formed in the annuli. The flowrate required to suspend the particles or transport the particles in the rolling mechanism was found to increase with an increase in the inclination angle and the gradient of this increase was greater for the two-phase flow than that of the single-phase flow.

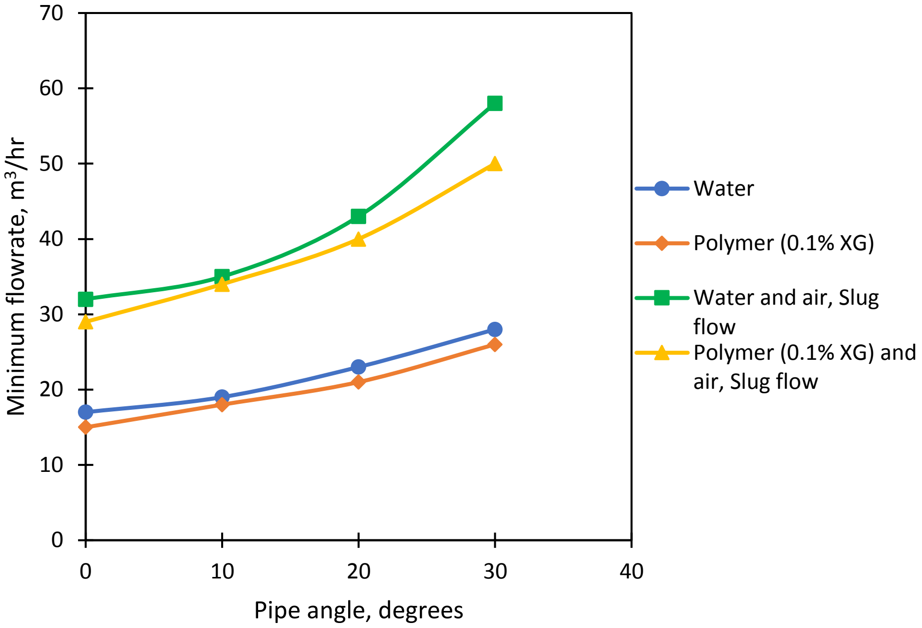

Fig. 10. Effect of inclination angle on particle transport in the concentric annuli

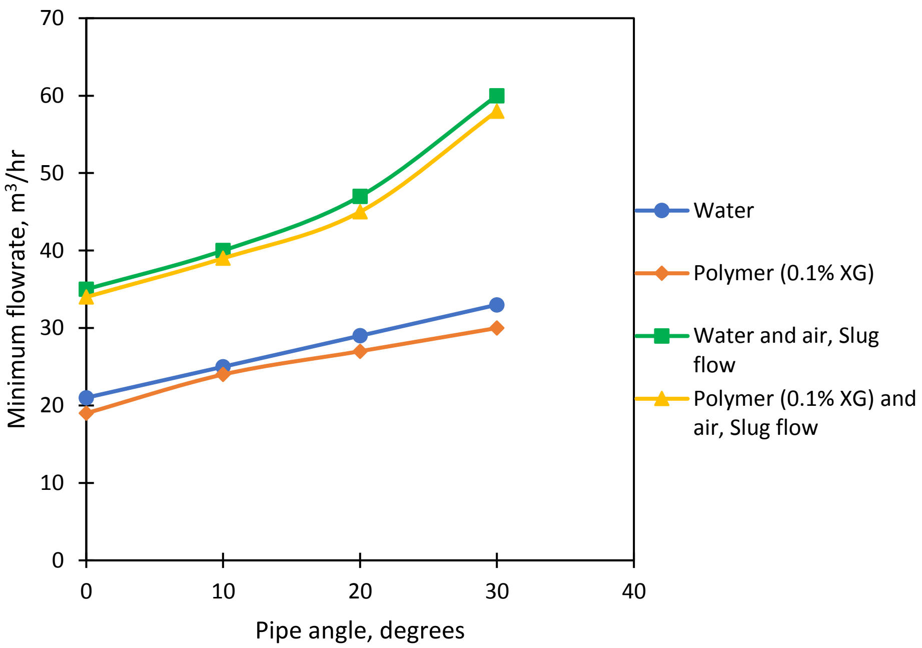

Fig. 11. Effect of inclination angle on particle transport in the eccentric annuli

An example of the particle transport mechanism for the slug flow pattern in the horizontal and inclined annuli sections is shown in Fig.A.5. It was observed that at a certain air-liquid flowrate, the particles in the horizontal test sections were being transported predominantly as a moving bed at the bottom of the annuli while a relatively high stationary bed is formed at the bottom of the inclined annuli test sections and increased over time. One of the main reasons for the formation of a stationary bed in the inclined annulus is the change in the local mixture properties of the fluid in the annulus which alters the forces acting on the particles. This makes it harder to transport cuttings in an upward inclined flow when the slug flow pattern is existing in the wellbore annuli.

4.3 Eccentricity

Generally, it was observed that the height of the stationary bed formed in the eccentric annuli was higher than that formed for the same fluid flowrates in the concentric annuli and for all the fluid types investigated. In some test conditions where a moving bed or no bed was formed in concentric annuli, a stationary bed was formed in the eccentric annuli for the single-phase and two-phase flows. With all things being equal and no external influence, the test results showed that it is easier to clean the concentric annuli when compared to the eccentric annuli. For the test conditions investigated, eccentricity affected the particle transport efficiency under the two-phase gas-liquid flow conditions more than the single-phase flow conditions.

4.4 Inner pipe rotation

In the experimental test for two-phase flow in the concentric and eccentric annuli test sections, the increase of the inner pipe rotation did not lead to a transition of the prevailing flow pattern for both the Newtonian and non-Newtonian fluid types. The fluid flow pattern formed in the annulus was mainly a function of the fluid properties and the gas/liquid flowrates and due to the turbulent nature of two-phase flow, the inner pipe rotation of up to a maximum of 150 rpm could not generate enough tangential force to overcome the axial force of the flow. From the experimental study of the effect of inner pipe rotation on the movement of the particles, it was observed that the effect of the inner pipe rotation on the cuttings transport mechanism was dependent on the fluid rheology, the flow pattern and the inclination angle of the annulus. In the horizontal concentric annuli sections, the increase in the rotary speed of the inner pipe produced a little or no decrease in the height or area of the stationary bed for both the Newtonian and non-Newtonian single-phase and two-phase fluids. The height of the bed formed in the annulus was not reduced by the rotation of the inner pipe for all the investigated flow patterns in the horizontal concentric annuli test section (Fig. 12).

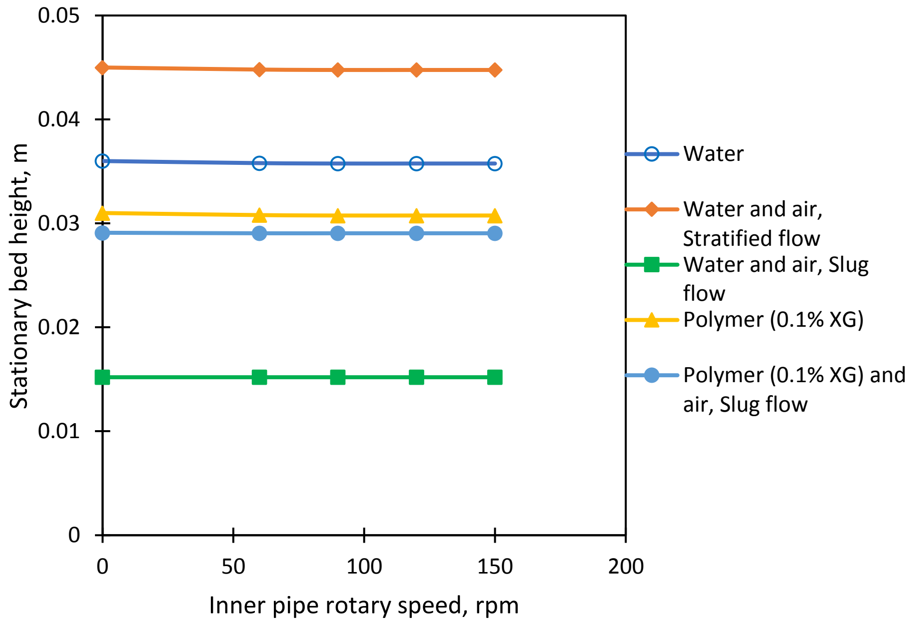

Fig. 12. Effect of inner pipe rotation on bed thickness in horizontal concentric annuli

The effect of the inner pipe rotation on the particle transport for the flow of the different fluid types in the inclined annulus is shown in Fig. 13. It was observed that the inner pipe rotation had little or no influence on the area or thickness of the stationary bed formed in the inclined annuli test sections for the two-phase flow fluid types. However, for the single-phase fluids, an increase in the inner pipe rotary speed led to a significant decrease in the thickness of the stationary bed.

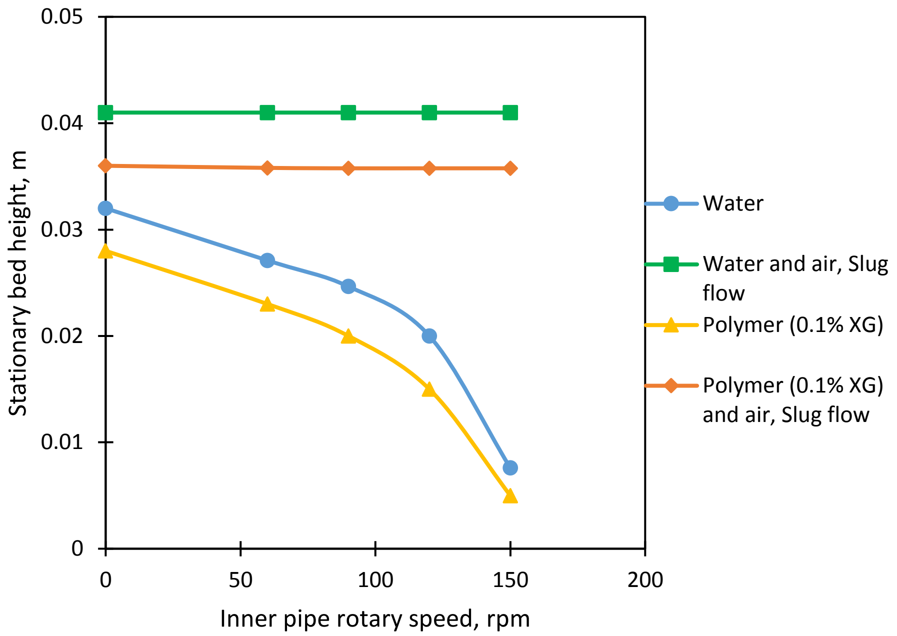

Fig. 13. Effect of inner pipe rotation on bed thickness in inclined concentric annuli

Fig.A.6a shows the effect of inner pipe rotation on the clearing of a stationary bed formed in the 20° inclined annulus test section flowing with a single-phase fluid. It can be seen that with change in time, the transport mechanism of the particles was transformed from the stationary bed regime and the particles were transported in the suspension and moving bed mechanism. Fig.A.6b shows the effect of the inner pipe rotation on the particles in the two-phase flow with the slug flow pattern in the inclined annulus. The increase in the inner pipe rotary speed had little or no significant influence on the size or thickness of the stationary bed formed in the annulus. The effect of the inner pipe rotation on the transport of the particles is a lot more significant in the eccentric annulus. However, the degree of the effect of rotation is highly dependent on the fluid rheology, fluid flow pattern and the angle of inclination of the annuli. For the horizontal eccentric annuli (Fig. 14), the height of the stationary bed reduced significantly with the increase in the rotary speed of the inner pipe. The particles in the single-phase flow responded a lot better to the inner pipe rotation than the particles in the two-phase flow and the fluids with the non-Newtonian rheology generally performed better than the Newtonian fluids especially for the single-phase flows.

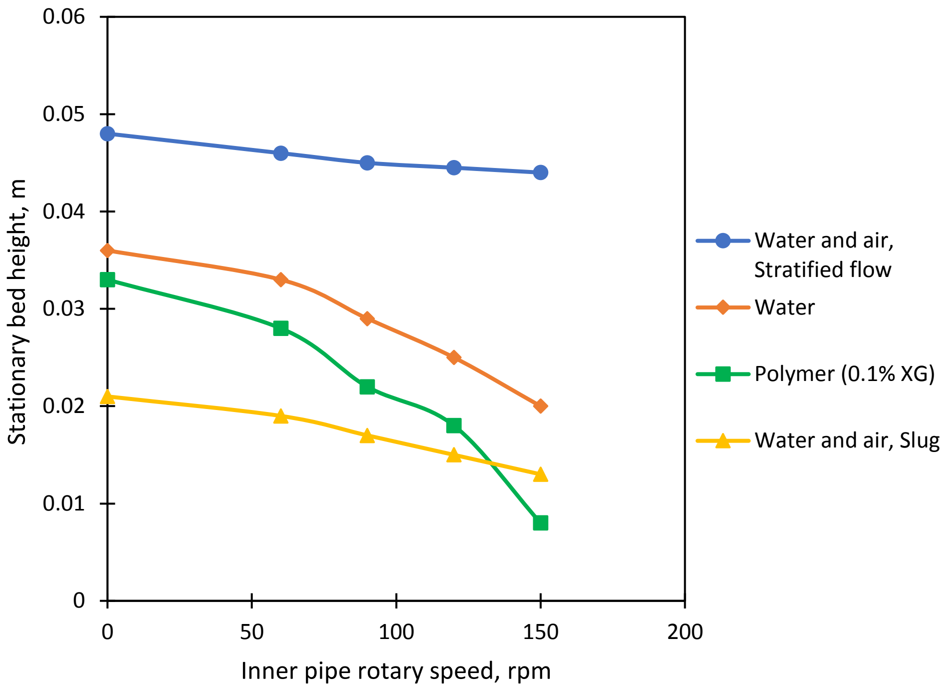

Fig. 14: Effect of inner pipe rotation on bed thickness in horizontal eccentric annuli

Fig. 15 shows the impact of the inner pipe rotation on the particles in the inclined eccentric annuli. It can be seen that the impact of the inner pipe rotation is a lot more significant in terms of the reduction of the stationary bed for the single-phase fluids. However, for the two-phase fluids, the stationary bed is just slightly reduced with the increase in inner pipe rotation.

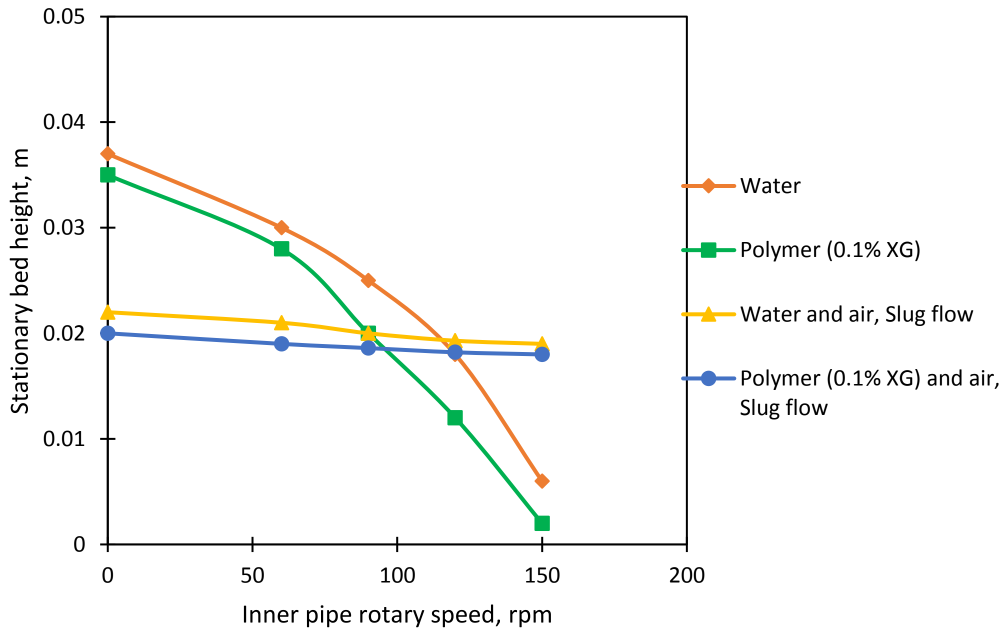

Fig. 15: Effect of inner pipe rotation on bed thickness in inclined eccentric annuli

4.5 Annuli pressure gradient

The annuli pressure gradient of fluid flow with entrained solid particles is significantly higher than the pressure gradient when no solid particles are transported in the flow. The prevailing cuttings transport mechanism and the properties of the particles and the fluid have a significant influence on the pressure gradient in the annuli. If the fluid flowrate generates an annuli average velocity that is below the MTV required to keep the particles in suspension, the particle would fall towards the bottom of the annuli and be transported as a moving bed. A stationary bed is however, formed if the average fluid velocity falls below the MTV required for the particles to roll or slide at the bottom wall of the annuli. If a stationary bed exists in the annuli, the flow area is reduced, and the fluid is forced to flow in the reduced flow area above the bed. With the flowrate being constant, this leads to an increase in the average velocity of the fluid, increased wall and fluid to bed interfacial shear stresses and a corresponding increase in the annuli pressure gradient. Fig. 16 shows the difference between the signals generated by the differential pressure transducers when a stationary bed is present and when no bed is present in the annulus. It can be seen that the real-time differential pressure measured when a stationary bed is present in the annulus is significantly higher than that obtained when no stationary bed is present in the annulus. Even though the stationary bed increases the annuli pressure gradient, the pressure gradient is still highly dependent on the gas-liquid flow pattern, fluid and particle properties and the existing particle transport mechanism in the annuli.

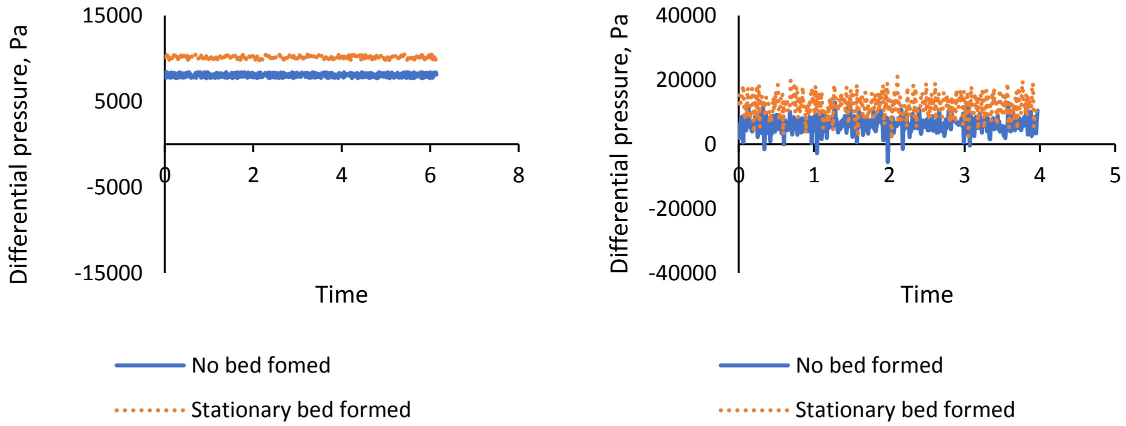

(a) (b)

Fig. 16: Real-time annuli differential pressure for (a) single-phase flow (water) and (b) two-phase slug flow (water and air)

The suspension, moving bed and the stationary bed particle transport mechanism can exist either individually or simultaneously in the annuli irrespective of the gas-liquid fluid flow pattern. However, the particle vertical concentration is highly dependent on the gas-liquid fluid flow pattern. The stationary bed height predicted by the model was compared to the recorded stationary bed height data that were obtained from experimental tests involving the flow of single-phase and two-phase fluids with solid particles in the annuli (Fig. 17 and Fig. 18). There is a favourable agreement between the predicted and measured stationary bed height with a maximum error of about ±16%.

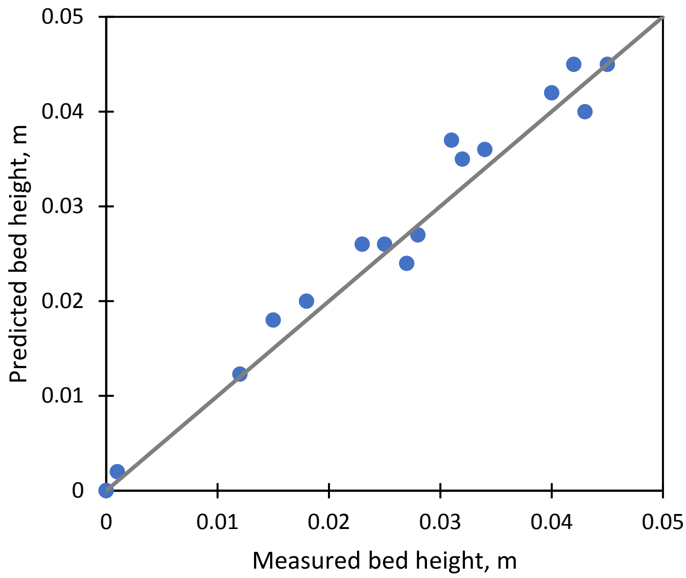

Fig. 17: Stationary bed height model performance for the annuli flow of water and water and air

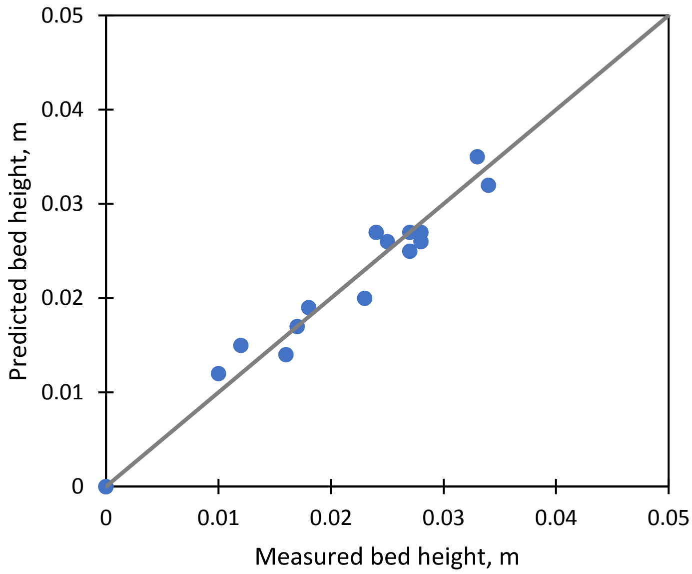

Fig. 18: Stationary bed height model performance for the annuli flow of polymer and polymer and air

The comparison of the pressure gradient obtained from the experimental tests and the pressure gradient calculated from the multi-layered cutting transport model for all the investigated gas-liquid fluid flow patterns, fluid types and the different particle transport mechanisms without inner pipe rotation are presented in Fig. 19 and Fig. 20. The positive results obtained from the comparison of the predicted pressure gradient to the measured pressure gradient validates the mathematical model. The maximum error margin is about ±20% for results obtained for the two-phase water and air fluids. However, the results obtained for the two-phase polymer and air fluids has an error of about ±30%. It is suspected that this relatively larger error was produced because the polymer solution is a non-Newtonian fluid and the friction factor equation used in this study was developed for Newtonian annuli fluid flow. A friction factor equation developed for non-Newtonian fluid flow in the annuli would have to be applied to improve the accuracy for predictions involving non-Newtonian fluids.

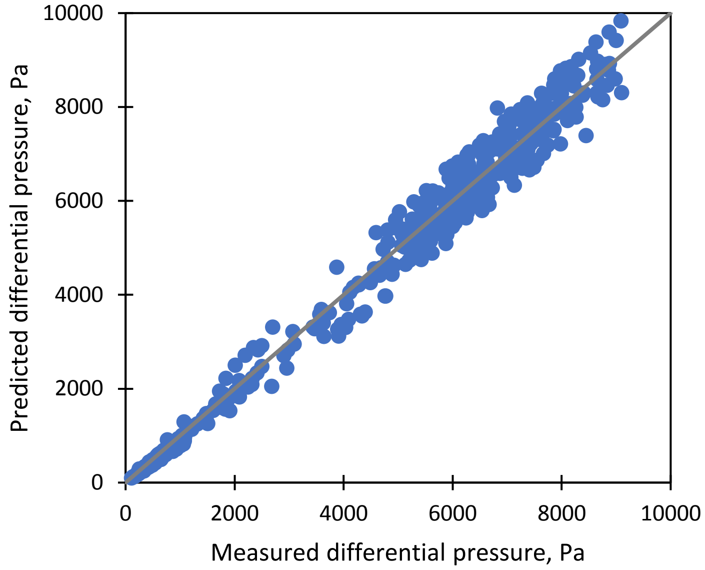

Fig. 19: Model performance for the annuli differential pressure (water and air)

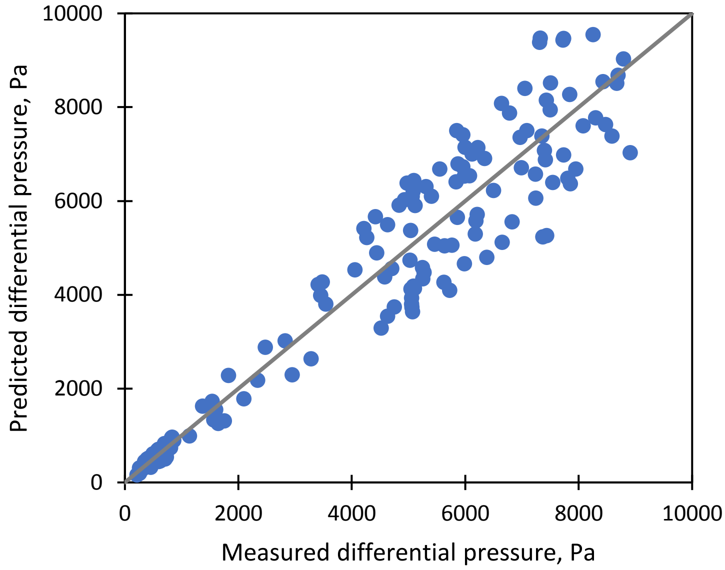

Fig. 20: Model performance for the annuli differential pressure (polymer and air)

5.0 Conclusions

In this study, an experimental investigation was carried out to investigate the effect of two-phase gas-liquid fluid flow patterns on wellbore hydraulics and cuttings transport efficiency for UBD operations. A unique experimental setup was used to visualise and capture relevant data concerning various gas-liquid fluid flow patterns flowing with and without solid particles in the concentric and eccentric annuli with and without inner pipe rotation. New flow pattern dependent mathematical multi-layered models and several equations were developed to predict the cutting transport mechanism, determine the stationary bed height and calculate the wellbore pressure losses along with other relevant information for the annuli flow of two-phase gas-liquid fluids. The models presented in this study are valid for any level of eccentricity and can be applied for both horizontal and inclined annuli flows. The performance of the models have been validated with the experimental results which shows favourable agreeement. The following conclusions have been drawn from this study:

1. The drilling fluid flowrate is the most important parameter that influences cuttings transport efficiency during drilling operations. However, for UBD operations, the prevailing gas-liquid fluid flow pattern must be taken into account in order to accurately determine the optimal flowrate for effective hole cleaning.
2. The requirements to clean the eccentric annuli are higher than that required for the concentric annuli for both single-phase and two-phase Newtonian or non-Newtonian fluids. Thus, it is easier to clean the concentric annuli than the eccentric annuli when there is no external or mechanical influence.
3. For drilling operations involving the flow of gas-liquid two-phase fluids in the annuli, the liquid phase plays a more significant role in the movement of the cuttings irrespective of the gas-liquid fluid flow pattern. Thus, the properties of the liquid phase is an important factor for effective cuttings transport.
4. Effective hole cleaning is dependent on the wellbore inclination angle. However, under UBD conditions, the degree of this effect is highly dependent on the fluid properties and gas-liquid flow pattern. The wellbore inclination angle influences the local mixture properties of the fluids in the annuli which as a result affects the cutting transport efficiency and wellbore hydraulics.
5. For a fully developed slug flow with or without the presence of cuttings, the liquid film length and thus the fluid mixture properties are dependent on the wellbore inclination angle.
6. An increase in the cuttings stationary bed height increases the annuli pressure losses for all the fluid types and gas-liquid flow patterns. Thus, if the inner pipe rotation decreases the stationary bed height it also leads to a corresponding decrease in the annuli pressure losses.
7. The effect of the inner pipe rotation on cuttings transport efficiency for UBD is highly dependent on the flow pattern, fluid rheological properties, and the wellbore inclination angle amongst other important drilling parameters.
8. There is little or no effect of drillpipe rotation on cuttings transport in the horizontal concentric annuli for both single-phase and two-phase fluids under the conditions investigated. However, in the inclined concentric annuli drillpipe rotation can improve cuttings transport especially when using single-phase drilling fluids. In the horizontal and inclined eccentric annuli, drillpipe rotation can improve cuttings transport for both single-phase and two-phase flows but generally the effect of the drillpipe rotation on two-phase flow for cutting transport is much less than that of the single-phase flow.

Data availability

The datasets generated during and/or analysed during the current study are available from the corresponding author upon request.

Acknowledgement

The authors are grateful to the School of Engineering at Robert Gordon University for facilitating and supporting this research work.

Conflict of interest

The authors declare that there is no conflict of interest.

801 **Nomenclature**

A	=	Cross-sectional area
B_1, B_2, B_3	=	Empirical constants
C	=	Cutting concentration
C_D	=	Coefficient of drag
C_L	=	Coefficient of lift
$\partial P/\partial L$	=	Pressure gradient
d_c	=	Cuttings size
d_e	=	Distance between the centre of the outer pipe and the inner pipe
d_2	=	Inner diameter of casing or wellbore
d_1	=	Outer diameter of drillpipe
d_x	=	Distance between the drillpipe and the casing wall at the lowest side
e	=	Wellbore eccentricity
F_B	=	Buoyancy force
F_D	=	Drag force
F_G	=	Gravitational force
F_L	=	Lift force
f_s	=	Coefficient of friction
f	=	Friction factor
g	=	Acceleration due to gravity
h	=	Height
H	=	Hold up
K_a	=	Pipe diameter ratio
L	=	Length
Q	=	Volumetric flowrate
S	=	Wetted perimeter
V	=	Average velocity
v	=	Relative velocity
$X1, X2, X3$	=	Functions for cross-sectional area calculations
β	=	Inclination angle between the vertical and wellbore flow axis
ρ	=	Density
τ	=	Shear stress
η	=	Ordinate in the complex plane
μ	=	Viscosity
λ	=	No-slip hold up
θ	=	Annulus inclination angle

Subscripts

a	=	Annulus
b	=	Stationary cuttings bed
c	=	Cuttings
1	=	Layer 1
2	=	Layer 2
3	=	Layer 3
f	=	Fluid
G	=	Gas
Gf	=	Gas in the liquid-film/gas pocket region
Gs	=	Gas in the slug body
L	=	Liquid
Lf	=	Liquid in the liquid-film/gas pocket region
Lf0	=	Starting position of the liquid film

LfA	=	Cuttings-fluid mixture in the liquid-film/gas pocket region
Lfc	=	Liquid-cuttings mixture in the liquid film
Ls	=	Liquid in the slug body
m	=	Gas-liquid mixture
MB	=	Moving bed
MR	=	Minimum for rolling bed
p	=	Drillpipe wall
s	=	Slug body
T	=	Translational
u	=	Slug unit
w	=	Annuli wall
x, y	=	Cartesian coordinate axes

References

Akhshik, S., Behzad, M., Rajabi, M., 2015. CFD–DEM approach to investigate the effect of drill pipe rotation on cuttings transport behavior. J. Pet. Sci. Eng. 127. https://doi.org/10.1016/j.petrol.2015.01.017

Akhshik, S., Rajabi, M., 2018. CFD-DEM modeling of cuttings transport in underbalanced drilling considering aerated mud effects and downhole conditions. J. Pet. Sci. Eng. 160. https://doi.org/10.1016/j.petrol.2017.05.012

Bilgesu, H.I., Ali, M.W., Aminian, K., Ameri, S., 2002. Computational fluid dynamics (CFD) as a tool to study cutting transport in wellbores, in: SPE Eastern Regional Meeting. Society of Petroleum Engineers. https://doi.org/10.2118/78716-MS

Caetano, E.F., Shoham, O., Brill, J.P., 1992. Upward vertical two-phase flow through an annulus—Part II: Modeling bubble, slug, and annular flow. J. Energy Resour. Technol. 114. https://doi.org/10.1115/1.2905916

Cayeux, E.., Mesagan, T.., Tanripada, S.., Zidan, M.., Fjelde, K.K.. K., 2014. Real-time evaluation of hole-cleaning conditions with a transient cuttings-transport model. SPE Drill. Complet. 29. https://doi.org/10.2118/163492-PA

Cho, H., Shah, S.N., Osisanya, S.O., 2001. Effects of fluid flow in a porous cuttings-bed on cuttings transport efficiency and hydraulics, in: SPE Annual Technical Conference and Exhibition. Society of Petroleum Engineers. https://doi.org/10.2118/71374-MS

Clark, R.K., Bickham, K.L., 1994. A mechanistic model for cuttings transport, in: SPE Annual Technical Conference and Exhibition. Society of Petroleum Engineers. https://doi.org/10.2118/28306-MS

Costa, S.S., Stuckenbruck, S., Fontoura, S.A.B., Martins, A.L., 2008. Simulation of transient cuttings transportation and ECD in wellbore drilling, in: Europec/EAGE Conference and Exhibition. Society of Petroleum Engineers. https://doi.org/10.2118/113893-MS

Doan, Q.T., Oguztoreli, M., Masuda, Y., Yonezawa, T., Kobayashi, A., Kamp, A., 2000. Modelling of transient cuttings transport in underbalanced drilling, in: IADC/SPE Asia Pacific Drilling Technology. Society of Petroleum Engineers. https://doi.org/10.2118/62742-MS

Doron, P., Barnea, D., 1993. A three-layer model for solid-liquid flow in horizontal pipes. Int. J. Multiph. Flow 19. https://doi.org/10.1016/0301-9322(93)90076-7

Duan, M., Miska, S.Z., Yu, M., Takach, N.E., Ahmed, R.M., Zettner, C.M., 2006. Transport of small cuttings in extended reach drilling, in: International Oil & Gas Conference and Exhibition in China. Society of Petroleum Engineers. https://doi.org/10.2118/104192-MS

Dukler, A.E., Hubbard, M.G., 1975. A model for gas-liquid slug flow in horizontal and near horizontal tubes. Ind. Eng. Chem. Fundam. 14. https://doi.org/10.1021/i160056a011

Dukler, A.E., Taitel, Y., 1986. Flow Pattern Transitions in Gas-Liquid Systems: Measurement and Modeling, in: Multiphase Science and Technology. Springer Berlin Heidelberg, Berlin, Heidelberg. https://doi.org/10.1007/978-3-662-01657-2_1

Erge, O., van Oort, E., 2020. Modeling cuttings transport and annular pack-off using local fluid velocities with the effects of drillstring rotation and eccentricity, in: IADC/SPE International Drilling Conference and Exhibition. Society of Petroleum Engineers. https://doi.org/10.2118/199587-MS

Fadairo, A., Ling, K., Rasouli, V., Adelakun, A., Tomomewo, O., 2020. An improved hydraulics model for aerated fluid underbalanced drilling in vertical wells. Upstream Oil Gas Technol. 5. https://doi.org/10.1016/j.upstre.2020.100009

Gao, E., Young, A.C., 1995. Hole cleaning in extended reach wells: Field experience and theoretical analysis using a pseudo-oil (acetal) based mud, in: SPE/IADC Drilling Conference. Society of Petroleum

Engineers. https://doi.org/10.2118/29425-MS

Gavignet, A.A., Sobey, I.J., 1989. Model aids cuttings transport prediction. J. Pet. Technol. 41. https://doi.org/10.2118/15417-PA

Gregory, G.A., Nicholson, M.K., Aziz, K., 1978. Correlation of the liquid volume fraction in the slug for horizontal gas-liquid slug flow. Int. J. Multiph. Flow 4. https://doi.org/10.1016/0301-9322(78)90023-X

Ibarra, R., Nossen, J., Tutkun, M., 2019. Two-phase gas-liquid flow in concentric and fully eccentric annuli. Part II: Model development, flow regime transition algorithm and pressure gradient. Chem. Eng. Sci. 203. https://doi.org/10.1016/j.ces.2019.02.021

Iyoho, A.W., 1980. Drilled cuttings transport by non-Newtonian drilling fluids through inclined, eccentric annuli. University of Tulsa, Tulsa, Oklahoma.

Kamp, A.M., Rivero, M., 1999. Layer modeling for cuttings transport in highly inclined wellbores, in: All Days. SPE. https://doi.org/10.2118/53942-MS

Li, M., Jv, Y.F., Wang, Z.Q., Hao, B.Y., Hong, Y.K., 2010. Simulation on the effect of drillstring rotation on hole cleaning for extended reach well. West-China Explor. Eng. 5, 51–54.

Li, Y., Bjorndalen, N., Kuru, E., 2007. Numerical modelling of cuttings transport in horizontal wells using conventional drilling fluids. J. Can. Pet. Technol. 46. https://doi.org/10.2118/07-07-TN

Li, Y., Kuru, E., 2004. Prediction of critical foam velocity for effective cuttings transport in horizontal wells, in: SPE/ICoTA Coiled Tubing Conference and Exhibition. Society of Petroleum Engineers. https://doi.org/10.2118/89324-MS

Lim, S.N., Khalil, M., Mohamed Jan, B., Si Ali, B., 2015. Lightweight biopolymer drilling fluid for underbalanced drilling: An optimization study. J. Pet. Sci. Eng. 129. https://doi.org/10.1016/j.petrol.2015.03.006

Luo, Y., 1988. Non-Newtonian annular flow and cuttings transport through drilling annuli at various angles. Heriot-Watt University, Edinburgh, Scotland.

Luo, Y., Bern, P.A., Chambers, B.D., 1992. Flow-rate predictions for cleaning deviated wells, in: IADC/SPE Drilling Conference. Society of Petroleum Engineers. https://doi.org/10.2118/23884-MS

Ma, T., Chen, P., Zhao, J., 2016. Overview on vertical and directional drilling technologies for the exploration and exploitation of deep petroleum resources. Geomech. Geophys. Geo-Energy Geo-Resources 2. https://doi.org/10.1007/s40948-016-0038-y

Masuda, Y., Doan, Q., Oguztoreli, M., Naganawa, S., Yonezawa, T., Kbayashi, A., Kamp, A., 2000. Critical cuttings transport velocity in inclined annulus: Experimental studies and numerical simulation, in: SPE/CIM International Conference on Horizontal Well Technology. Society of Petroleum Engineers. https://doi.org/10.2118/65502-MS

Mousavi, H., Mostafavi, V., Nazari, T., Hareland, G., Shirkavand, F., 2008. Modeling of three-phase flow in the annuli during directional UBD operations, in: SPE International Symposium and Exhibition on Formation Damage Control. Society of Petroleum Engineers. https://doi.org/10.2118/112679-MS

Mukherjee, H., Brill, J.P., 1985. Pressure drop correlations for inclined two-phase flow. J. Energy Resour. Technol. 107. https://doi.org/10.1115/1.3231233

Okrajni, S., Azar, J.J., 1986. The effects of mud rheology on annular hole cleaning in directional wells. SPE Drill. Eng. 1. https://doi.org/10.2118/14178-PA

Ostroot, K., Shayegi, S., Zoontjes, D., Lovorn, R., 2007. Comparison and advantages of underbalanced and managed-pressure drilling techniques: When should each be applied?, in: All Days. OTC.

https://doi.org/10.4043/18561-MS

Oyeneyin, B., 2015. Integrated Sand Management For Effective Hydrocarbon Flow Assurance, 1st ed, Developments in Petroleum Science. Elsevier.

Ozbayoglu, E.M., Miska, S.Z., Reed, T., Takach, N., 2003. Cuttings transport with foam in horizontal & highly-inclined wellbores, in: SPE/IADC Drilling Conference. Society of Petroleum Engineers. https://doi.org/10.2118/79856-MS

Ozbayoglu, M.E., Saasen, A., Sorgun, M., Svanes, K., 2007. Estimating critical velocity to prevent bed development for horizontal-inclined wellbores, in: SPE/IADC Middle East Drilling and Technology Conference. Society of Petroleum Engineers. https://doi.org/10.2118/108005-MS

Pandya, S., Ahmed, R., Shah, S., 2020. Wellbore cleanout in inclined and horizontal wellbores: The effects of flow rate, fluid rheology, and solids density. SPE Drill. Complet. 35. https://doi.org/10.2118/194240-PA

Peden, J.M., Ford, J.T., Oyeneyin, M.B., 1990. Comprehensive experimental investigation of drilled cuttings transport in Inclined wells including the effects of rotation and eccentricity, in: European Petroleum Conference. Society of Petroleum Engineers. https://doi.org/10.2118/20925-MS

Sun, X., Wang, K., Yan, T., Shao, S., Jiao, J., 2014. Effect of drillpipe rotation on cuttings transport using computational fluid dynamics (CFD) in complex structure wells. J. Pet. Explor. Prod. Technol. 4. https://doi.org/10.1007/s13202-014-0118-x

Taitel, Y., Barnea, D., 1990. Two-Phase Slug Flow. https://doi.org/10.1016/S0065-2717(08)70026-1

Verma, C., Rodriguez, F., Qasin, Q.M., Chaaouri, A.M., Akel, S., Akiki, G., Afolabi, J., 2017. Drilling optimisation of extended reach multilateral wells to maximise reservoir contact in carbonate, in: Day 2 Wed, October 18, 2017. SPE. https://doi.org/10.2118/186982-MS

Wang, Z., Zhai, Y., Hao, X., Guo, X., Sun, L., 2010. Numerical simulation on three layer dynamic cutting transport model and its application on extended reach drilling, in: IADC/SPE Asia Pacific Drilling Technology Conference and Exhibition. Society of Petroleum Engineers. https://doi.org/10.2118/134306-MS

Wei, N., Meng, Y., Li, G., Wan, L., Xu, Z., Xu, X., Zhang, Y., 2013. Cuttings transport models and experimental visualization of underbalanced horizontal drilling. Math. Probl. Eng. 2013. https://doi.org/10.1155/2013/764782

Xiao, J.J., Shonham, O., Brill, J.P., 1990. A comprehensive mechanistic model for two-phase flow in pipelines, in: SPE Annual Technical Conference and Exhibition. Society of Petroleum Engineers. https://doi.org/10.2118/20631-MS

Zhang, F., Wang, Yidi, Wang, Yuezhi, Miska, S., Yu, M., 2020. Modeling of dynamic cuttings transportation during drilling of oil and gas wells by combining 2D CFD and 1D discretization approach. SPE J. 25. https://doi.org/10.2118/199902-PA

Zhang, H.-Q., Wang, Q., Sarica, C., Brill, J.P., 2003. A unified mechanistic model for slug liquid holdup and transition between slug and dispersed bubble flows. Int. J. Multiph. Flow 29. https://doi.org/10.1016/S0301-9322(02)00111-8

Appendix A

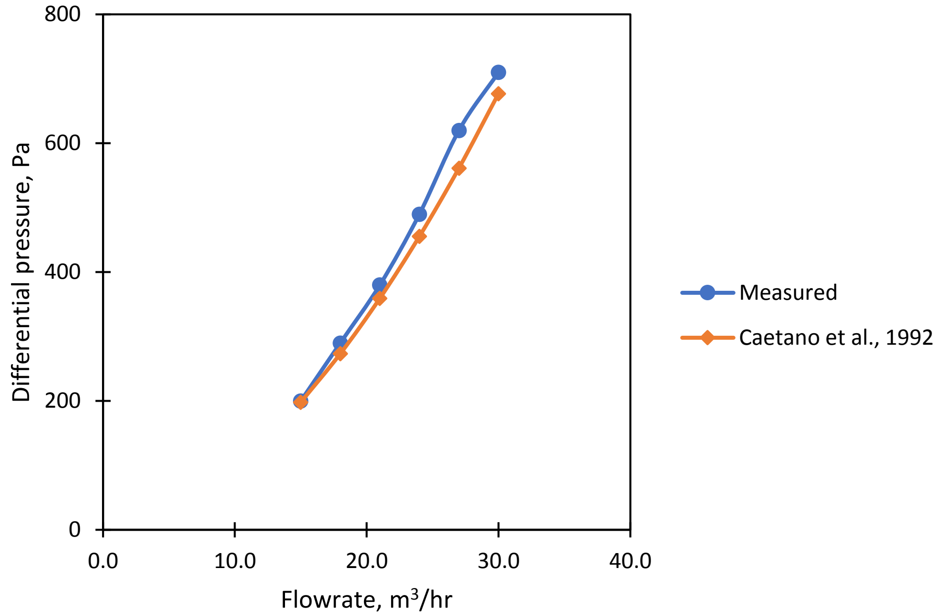

Fig.A.1: Comparison of the differential pressure obtained from the experimental rig to that which is calculated using the model suggested by Caetano et al. (1992)

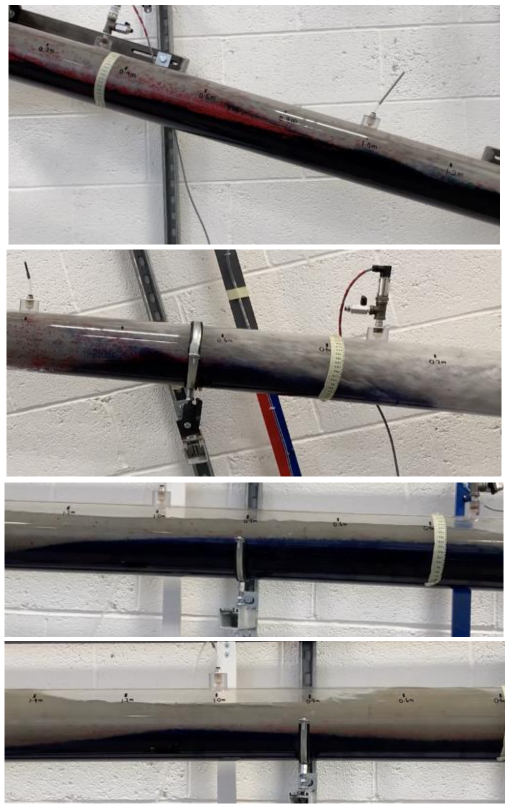

(a) Single-phase flow

(b) Dispersed bubble flow

(c) Stratified flow

(d) Slug flow horizontal

Fig.A.2: Examples of different cutting transport mechanisms existing in the different gas-liquid flow patterns

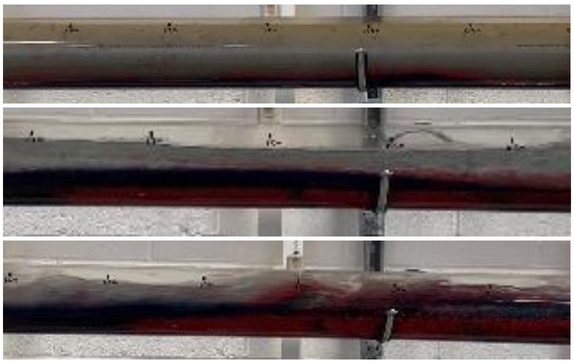

(a) Single-phase flow, $Q = 30\ m^3/hr$

(b) Stratified flow, $Q_m = 35\ m^3/hr$

(c) Slug flow, $Q_m = 42\ m^3/hr$

$$Q_m = Q_L + Q_G$$

Fig.A.3: Flow pattern with different gas-liquid input flowrates

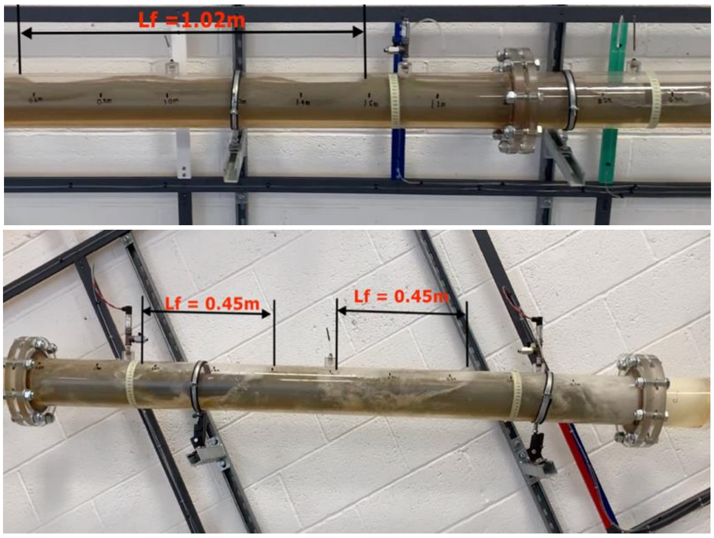

(a) Horizontal

(b) 20^0 Inclined

Fig.A.4: Liquid film length and fluid distribution a fully developed slug flow in a horizontal and inclined annulus

Fig.A.5: Comparison of particle transport in the horizontal and inclined annuli for water and air (top) moving bed with slug flow pattern in the horizontal annulus and (bottom) stationary bed for the slug flow pattern in 30^o inclined annulus

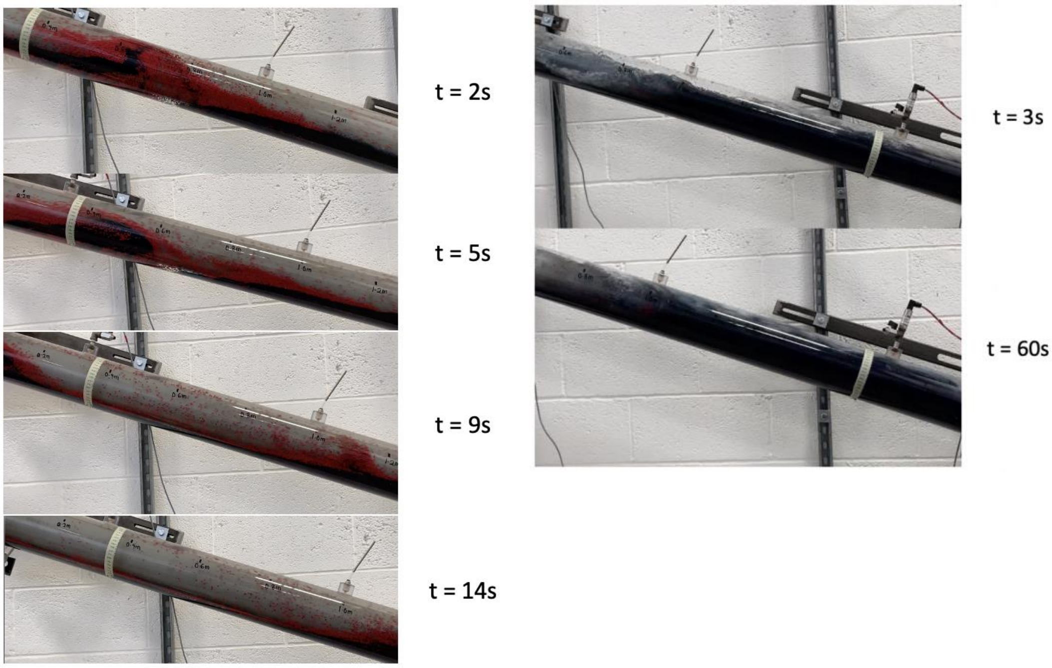

(a) (b)

Fig.A.6: Effect of inner pipe rotation at 150 rpm on particle transport in inclined concentric annuli for (a) single-phase flow (water) and (b) two-phase slug flow (water and air)

Appendix B

Friction factor:

The calculation of the shear stresses in the mathematical models for each of the flow patterns require the determination of the wall and interfacial friction factors. The wellbore and drillpipe wall friction factors for the concentric and eccentric annuli can be determined using the models suggested by Ibarra et al. (2019). The interfacial friction factors may be determined as follows:

Gas-liquid interface:

$$\frac{1}{\sqrt{f_i}} = 3.48 - 4\log\left[\frac{\gamma(V_i - V_{i+1})^2 f_i}{gD_{hi}} + \frac{9.35}{Re_i\sqrt{f_i}}\right] \qquad \text{Eq. (B.1)}$$

$\gamma = 0.1 - 0.5$

Suspension-moving bed interface:

$$\frac{1}{\sqrt{2f_i}} = -0.86\ln\left[\frac{\frac{d_p}{D_{hi}}}{3.7} + \frac{2.51}{Re_i\sqrt{2f_i}}\right] \qquad \text{Eq. (B.2)}$$

Moving bed-stationary bed:

$$f_i = \frac{0.046}{Re_i^{\,0.2}} \qquad \text{Eq. (B.3)}$$

Hydraulic diameters and Reynolds number:

Layer 1:

$$D_{h1} = \frac{4A_1}{S_{1w} + S_{1p} + S_{12}} \quad Re_1 = \frac{\rho_1 V_1 D_{h1}}{\mu_1} \qquad \text{Eq. (B.4)}$$

Layer 2:

$$D_{h2} = \frac{4A_2}{S_{2w} + S_{2p} + S_{23}} \quad Re_2 = \frac{\rho_2 V_2 D_{h2}}{\mu_2} \qquad \text{Eq. (B.5)}$$

Layer 3:

$$D_{h3} = \frac{4A_3}{S_{3w} + S_{34} + S_{3p}} \quad Re_2 = \frac{\rho_3 V_3 D_{h3}}{\mu_3} \qquad \text{Eq. (B.6)}$$

Appendix C

Geometric and closure relationships

Dispersed bubble flow:

$$d_x = \frac{d_2}{2} - \left(\frac{2d_c + d_1}{2}\right) \qquad \text{Eq. (C.1)}$$

$$S_{12} = d_2 \sin\left[\cos^{-1}\left(\frac{d_2 - 2h_2}{d_2}\right)\right] - d_1 \sin\left[\cos^{-1}\left(\frac{d_1 - 2(h_2 - d_x)}{d_1}\right)\right] \qquad \text{Eq. (C.2)}$$

$$S_{23} = d_2 \sin\left[\cos^{-1}\left(\frac{d_2 - 2h_b}{d_2}\right)\right] - d_1 \sin\left[\cos^{-1}\left(\frac{d_1 - 2(h_b - d_x)}{d_1}\right)\right] \qquad \text{Eq. (C.3)}$$

$$S_{1p} = \pi d_1 - d_1 \cos^{-1}\left(\frac{d_1 - 2(h_2 - d_x)}{d_1}\right) \qquad \text{Eq. (C.4)}$$

$$S_{1w} = \pi d_2 - d_2 \cos^{-1}\left(\frac{d_2 - 2h_2}{d_2}\right) \qquad \text{Eq. (C.5)}$$

$$S_{3w} = d_2 \cos^{-1}\left(\frac{d_2 - 2h_b}{d_2}\right) \qquad \text{Eq. (C.6)}$$

$$S_{3p} = d_1 \cos^{-1}\left(\frac{d_1 - 2(h_b - d_x)}{d_1}\right) \qquad \text{Eq. (C.7)}$$

$$S_{2w} = \pi d_2 - S_{1w} - S_{3w} \qquad \text{Eq. (C.8)}$$

$$S_{2p} = \pi d_1 - S_{1p} - S_{3p} \qquad \text{Eq. (C.9)}$$

Stratified flow:

$$S_{12} = d_2 \sin\left[\cos^{-1}\left(\frac{d_2 - 2h_2}{d_2}\right)\right] - d_1 \sin\left[\cos^{-1}\left(\frac{d_1 - 2(h_2 - d_x)}{d_1}\right)\right] \qquad \text{Eq. (C.10)}$$

$$S_{23} = d_2 \sin\left[\cos^{-1}\left(\frac{d_2 - 2h_1}{d_2}\right)\right] - d_1 \sin\left[\cos^{-1}\left(\frac{d_1 - 2(h_1 - d_x)}{d_1}\right)\right] \qquad \text{Eq. (C.11)}$$

$$S_{34} = d_2 \sin\left[\cos^{-1}\left(\frac{d_2 - 2h_b}{d_2}\right)\right] - d_1 \sin\left[\cos^{-1}\left(\frac{d_1 - 2(h_b - d_x)}{d_1}\right)\right] \qquad \text{Eq. (C.12)}$$

$$S_{1p} = \pi d_1 - d_1 \cos^{-1}\left(\frac{d_1 - 2(h_2 - d_x)}{d_1}\right)$$ Eq. (B.13)

$$S_{1w} = \pi d_2 - d_2 \cos^{-1}\left(\frac{d_2 - 2h_2}{d_2}\right)$$ Eq. (B.14)

$$S_{3w} = d_2 \cos^{-1}\left(\frac{d_2 - 2h_1}{d_2}\right) - S_{4w}$$ Eq. (B.15)

$$S_{4w} = d_2 \cos^{-1}\left(\frac{d_2 - 2h_b}{d_2}\right)$$ Eq. (C.16)

$$S_{3p} = d_1 \cos^{-1}\left(\frac{d_1 - 2(h_1 - d_x)}{d_1}\right) - S_{4p}$$ Eq. (C.17)

$$S_{4p} = d_1 \cos^{-1}\left(\frac{d_1 - 2(h_b - d_x)}{d_1}\right)$$ Eq. (C.18)

$$S_{2w} = \pi d_2 - S_{1w} - S_{3w} - S_{4w}$$ Eq. (C.19)

$$S_{2p} = \pi d_1 - S_{1p} - S_{3p} - S_{4p}$$ Eq. (C.20)

Slug flow:

$$\tau_{2w} = f_{2w} \frac{\rho_2 V_{Lf}|V_{Lf}|}{2}$$ Eq. (C.21)

$$\tau_{1w} = f_{1w} \frac{\rho_1 V_{Gf}|V_{Gf}|}{2}$$ Eq. (C.22)

$$\tau_{12} = f_{12} \frac{\rho_1 (V_{Gf} - V_{Lf})|V_{Gf} - V_{Lf}|}{2}$$ Eq. (C.23)

$$\tau_{2p} = \frac{f_{2p}\, \rho_2 V_{Lf}|V_{Lf}|}{2}$$ Eq. (C.24)

$$\tau_{1p} = \frac{f_{1p}\, \rho_1 V_{Gf}|V_{Gf}|}{2}$$ Eq. (C.25)

The following closure relationships were obtained from literature:
Length of slug body (Zhang et al., 2003)

$$L_s = (32\cos^2\theta + 16\sin^2\theta)D_h \qquad \text{Eq. (C.26)}$$

Translational velocity:

$$V_T = 1.2V_m + 0.54\sqrt{g\,D_{Ep}}\cos\theta + 0.345\sqrt{g\,D_{Ep}}\sin\theta \qquad \text{Eq. (C.27)}$$

where $D_{Ep} = d_1 + d_2$

Velocity of the gas in the slug body:

$$V_{Gs} = 1.2V_m + 1.53\left[\frac{(\rho_L - \rho_G)\,g\,\sigma}{\rho_L^2}\right]^{0.25} {H_{Ls}}^{0.5}\sin\theta \qquad \text{Eq. (C.28)}$$

Liquid hold-up in the slug body (Gregory et al., 1978)

$$H_{Ls} = \frac{1}{1 + \left(\frac{V_m}{8.66}\right)^{1.39}} \qquad \text{Eq. (C.29)}$$

Appendix D

Calculation procedure for the mathematical multi-layered models

Bubble and dispersed bubble flow:

1. Specify input parameters: Q_L, Q_G, ρ_L, ρ_G, ρ_c, C_c, μ_L, μ_G, σ, θ, d_1, d_2, e
2. Determine V_{MR} from Eq.3, where $d_x = 0.5(d_2 - d_1) - d_e$ and $\beta = \pi/2 - \theta$
3. Calculate V_m using $V_m = (Q_L + Q_G)/A_a$ and compare the value with V_{MR}. If $V_m < V_{MR}$, set $V_m = V_{MR}$
4. Calculate the area available for the fluid flow in the annuli, A_{flow} from $A_{flow} = (Q_L + Q_G)/V_m$ and calculate the area of the stationary bed, A_b from $A_b = A_a - A_{flow}$
5. Calculate the stationary bed height, h_b by solving Eq.18. If $h_b > 0$, move to step 7.
6. If $h_b = 0$, determine V_{MS} from Eq. 4. If $V_m \geq V_{MS}$ then move to step 7, noting that the particles are in homogeneous suspension and S_{12} and S_{23} are zero. However, if $V_m < V_{MS}$ then the suspension and moving bed layers are present and S_{23} is zero.
7. Simultaneously solve Eq.19, Eq.20, Eq.21 and Eq.22 to obtain the pressure gradient in the annuli. Other output parameters such as C_1, h_2 and V_2 would be available in the final iteration.

Stratified flow:

1. Specify input parameters: Q_L, Q_G, ρ_L, ρ_G, ρ_c, C_c, μ_L, μ_G, σ, θ, d_1, d_2, e
2. Determine V_{MR} from Eq.3, where $d_x = 0.5(d_2 - d_1) - d_e$ and $\beta = \pi/2 - \theta$
3. Calculate V_L from $V_L = Q_L/A_2$ by solving Eq.34 and Eq.35 and compare the value with V_{MR}. If $V_L < V_{MR}$, set $V_L = V_{MR}$. Note that V_L is calculated by assuming that cuttings are not present in the annuli (C_2 & $C_3 = 0$). Thus S_{3p}, S_{23}, S_{34} and S_{3w} are zero and h_2 represents the liquid height.
4. Calculate the area available for the liquid flow in the annuli, A_L from $A_L = Q_L/V_L$ and calculate the area of the stationary bed, A_b from $A_b = A_a - A_G - A_L$
5. Calculate the stationary bed height, h_b by solving Eq.18. If $h_b > 0$, move to step 7.
6. If $h_b = 0$, determine V_{MS} from Eq. 4. If $V_L \geq V_{MS}$ then move to step 7, noting that the particles are in homogeneous suspension in the liquid phase and S_{3p}, S_{23}, S_{34} and S_{3w} are zero. However, if $V_L < V_{MS}$ then the suspension and moving bed layers are present and S_{34} is zero.
7. Simultaneously solve Eq.32, Eq.33, Eq.34 to Eq.36 to obtain the pressure gradient in the annuli. Other output parameters such as C_2, h_1, h_2 and V_3 would be available in the final iteration.

Slug flow:

1. Specify input parameters: Q_L, Q_G, ρ_L, ρ_G, ρ_c, C_c, μ_L, μ_G, σ, θ, d_1, d_2, e
2. Determine V_{MR} from Eq.3, where $d_x = 0.5(d_2 - d_1) - d_e$ and $\beta = \pi/2 - \theta$
3. Calculate V_m using $V_m = (Q_L + Q_G)/A_a$ and compare the value with V_{MR}. If $V_m < V_{MR}$, set $V_m = V_{MR}$
4. Calculate the area available for the fluid flow in the annuli, A_{flow} from $A_{flow} = (Q_L + Q_G)/V_m$ and calculate the area of the stationary bed, A_b from $A_b = A_a - A_{flow}$
5. Calculate the stationary bed height, h_b by solving Eq.18.
6. Determine V_T, H_{Ls}, V_{Gs} from closure relationships (Eq.C.26 to Eq.C.29) and calculate V_{Ls} using $V_{Ls} = \left(V_m - V_{Gs}(1 - H_{Ls})\right)/H_{Ls}$.
7. Solve Eq.76 to obtain the liquid film height just behind the slug body region, h_{Lf0}
8. Calculate the length of the slug body L_s from Eq.C.26
9. Obtain the liquid film profile $h_{Lf}(L)$, liquid holdup $H_{Lf}(L)$ and the axial fluid velocity distributions $V_{Lf}(L)$ and $V_{Gf}(L)$ in the liquid/gas pocket region by numerically integrating Eq.74 from $h_{Lf}(L = 0) = h_{Lf0}$ until Eq.55 is satisfied, thereby yielding the length of the liquid film, $L = L_{Lf}$. The equations for the shear stresses in Eq.74 are given in Eq.C.21 to Eq.C.25 Note that if $h_b > 0$, then C_{Lf} is calculated according to Eq.81. However, if $h_b = 0$, then $C_{Lf} = 0.5$ is assumed.
10. Calculate the entire length of the slug unit, L_u from $L_u = L_s + L_{Lf}$
11. If $h_b = 0$, determine V_{MS} from Eq. 4. If $V_m \geq V_{MS}$ then move to step 7, noting that the particles are in homogeneous suspension in the slug body region and S_{12} and S_{23} are zero. However, if $V_m < V_{MS}$ then the suspension and moving bed layers are present in the slug body region and S_{23} is zero.
12. Simultaneously solve Eq.56, Eq.57, Eq.58 and Eq.59 to obtain the annuli pressure gradient in the slug body region, $(\partial P/\partial L)_s$. Other output parameters such as C_1, h_2 and V_2 would be available in the final iteration.
13. Calculate the average density of the cuttings-fluid mixture in the liquid-film/gas pocket region from Eq.77
14. Solve Eq.78 to determine the total pressure drop across the entire slug unit and calculate the annuli pressure gradient from Eq.79